Distinct and interdependent functions of three RING proteins regulate recombination during mammalian meiosis

Masaru Ito[1,2,5,*], Yan Yun[1,2], Dhananjaya S. Kulkarni[1,2], Sumit Sandhu[1,2], Briana Nuñez[1,3], Linya Hu[2], Kevin Lee[2], Nelly Lim[2], Rachel Hirota[2], Rowan Prendergast[2], Cynthia Huang[2], Ivy Huang[2] and Neil Hunter[1,2,4,5,6,*]

[1]Howard Hughes Medical Institute, University of California Davis, Davis, CA 95616, USA

[2]Department of Microbiology & Molecular Genetics, University of California Davis, Davis, CA 95616, USA

[3]Department of Biochemistry & Molecular Biology, Brown University, Providence, RI 02912, USA

[4]Department of Molecular & Cellular Biology, University of California Davis, Davis, CA 95616, USA

[5]Current address: Institute for Protein Research, Osaka University, Osaka 565-0871, Japan

[6]Lead contact: nhunter@ucdavis.edu (N.H.)

[*]Correspondence: msrito2@protein.osaka-u.ac.jp (M.I.), nhunter@ucdavis.edu (N.H.)

SUMMARY

Crossing-over between homologous chromosomes is essential for accurate segregation during meiosis. In mammals, factors required for crossing over include RNF212 and HEI10, RING-finger domain proteins implicated in modification by SUMO and ubiquitin, respectively. Here we show that a third RING protein, RNF212B, is essential for crossing over in mouse and characterize its relationships with RNF212 and HEI10. Mutant analysis indicates that, analogous to RNF212, RNF212B regulates recombination occurring in the context of synapsed chromosomes by stabilizing pro-crossover factors, regulating the progression of recombination, and enabling the differentiation and maturation of crossover-specific recombination complexes. Also, like RNF212, RNF212B localizes between synapsed chromosomes, initially as numerous foci along synaptonemal complexes (SCs) before undergoing HEI10-dependent redistribution to accumulate at prospective crossover sites. Despite these similarities, accumulation of RNF212B at nascent crossover sites is much greater than RNF212 and occurs earlier, coincident with the appearance of HEI10 foci, implicating concerted action of RNF212B and HEI10 in the differentiation of crossover sites. RNF212B localization also shows greater dependence on DNA double-strand breaks and SC formation than RNF212. Together, our analysis delineates three distinct but interdependent RING proteins that regulate meiotic recombination by integrating

signals from DSBs, synapsis, the cell-cycle, and developing crossover sites.

INTRODUCTION

During sexual reproduction, parents make equal genetic contributions to their offspring by producing gametes with precisely half the normal cellular ploidy. This is achieved via the two successive rounds of chromosome segregation that occur during meiosis. Accurate segregation during the first meiotic division (MI) requires crossing over between each pair of homologous chromosomes (homologs). In combination with cohesion between sister-chromatids, crossovers create connections called chiasmata that enable the stable biorientation of homolog pairs on the meiosis-I spindle [1-3]. Defective crossing over can trigger cell death via the spindle checkpoint [4], or cause aneuploidy due to chromosome missegregation [5,6], and is therefore associated with infertility, miscarriage, and congenital syndromes such as Down, Turner and Klinefelter [7-10].

Crossovers derive from the template-dependent chromosome repair process called homologous recombination, which is initiated by programmed DNA double-strand breaks (DSBs) formed during early meiotic prophase I [11]. DSBs are resected to create long 3' single-stranded tails that

assemble into nucleoprotein filaments comprising RecA-family proteins RAD51 and DMC1 and their accessory proteins [12]. Nucleoprotein filaments mediate homology search and DNA strand invasion to create a D-loop that can prime the local DNA synthesis required to repair the break [2]. Crossing over is generally the minority outcome of meiotic recombination with most breaks being repaired as noncrossovers without exchange of chromosome arms; for example, in mouse spermatocytes only ~24 crossovers are selected from ~250 DSBs [13]. At the DNA level, crossover and noncrossover pathways diverge after D-loop formation with crossover-destined events forming double-Holliday Junction intermediates (dHJs), which are resolved specifically into crossovers [14-16]. Noncrossovers form primarily via synthesis-dependent strand annealing in which the invading strand is extended by DNA synthesis and then displaced to anneal with the other DSB end and seal the break.

Meiotic recombination occurs in close physical and functional association with homolog axes, cohesin-based structures that organize sister-chromatids into linear arrays of chromatin loops [3]. In many species, including mammals, recombination mediates coalignment of homolog axes and their end-to-end connection by synaptonemal complexes (SCs), densely packed arrays of

transverse filaments that oligomerize between the axes [17]. Recombination is then completed in the context of the SC.

Crossover sites are selected from an excess of recombinational interactions in such a way that each pair of chromosomes almost always obtains at least one crossover, termed crossover assurance; adjacent events tend to be widely and evenly spaced via crossover interference (which also effectively limits total crossovers); and crossover numbers per nucleus show low variation relative to DSBs, a buffering process known as crossover homeostasis [2,3,18]. The molecular basis of crossover patterning remains unclear but manifests at the cytological level as the selective retention/accumulation of certain pro-crossover factors at designated crossover sites as prophase progresses [2,3]. Among these are RING-domain proteins related to budding yeast Zip3 [19], inferred to mediate protein modification by ubiquitin and the related small-protein modifier SUMO [2,20-27]. Species differ with respect to the number and subgroup (Zip3/RNF212 and HEI10) of Zip3-family members. For example, *Sordariales* and plant genomes encode a single HEI10 homolog [19,24,28]; *Drosophila* encodes three Zip3/RNF212-like proteins, two of which appear to be redundant [29 27]; and *C. elegans* has four members with homology to both subgroups

[25,26,30].

Mammalian genomes encode both RNF212 and HEI10 (a.k.a. CCNBIP1) homologs with interrelated functions that are essential for crossing over [21-23,31]. RNF212 specifically localizes to SCs, initially all along the central region as numerous small foci, before undergoing HEI10-dependent repatterning to accumulate at prospective crossover sites while being lost elsewhere [21-23]. RNF212 and other Zip3-family proteins are inferred to stabilize other pro-crossover factors that directly mediate the DNA events of crossing over [21-25,32,33]. These include the MutSγ complex, a heterodimer of MSH4 and MSH5 that can bind D-loops and Holliday junctions [15,16,34], and is inferred to stabilize and protect them from dissociation by the conserved Bloom-helicase/decatenase complex, BLM-TOPIIIα-RMI1-RMI2 (analogous to Sgs1-Top3-Rmi1 in budding yeast)[14,35-37]. In mouse spermatocytes, MutSγ initially localizes to a majority of recombination sites during late zygotene and early pachytene as homologs complete synapsis [13,21]. Subsequently, MutSγ is lost from most sites but retained at prospective crossover sites, which then accumulate crossover-maturation factors such as the MutLγ endonuclease [2,15].

Here we characterize RNF212B, a third mammalian Zip3-family member. Alleles of *Rnf212b* have been linked to heritable variation in crossover rate in cattle, Soay sheep, and red deer [38-41]; and a rare human *RNF212B* variant was recently associated with male infertility [42]. We show that mouse RNF212B undergoes crossover-specific patterning along SCs and is essential for crossing over and fertility in males and females. Differences in localization patterns and dynamics, phenotypes, and interdependencies imply that RNF212B, RNF212, and HEI10 function as distinct modules that integrate signals from DSBs, synapsis, the cell-cycle, and developing crossover complexes in order to effect the spatiotemporal coordination of the major events of meiotic prophase-I.

RESULTS

Mouse *Rnf212b* encodes a RING finger domain protein

The mouse *Rnf212b* gene located on chromosome 14 comprises 14 exons and encodes a 297 amino acid protein. The domain structure of the full-length RNF212B protein mirrors that of RNF212 with an N-terminal RING finger domain (36.7% amino-acid identity with RNF212), a ~70 amino acid region of predicted coiled-coil (25.7% identical) and a disordered serine-rich C-terminal tail (22.8% identical; **Figures 1A** and **S1A**). Expression from the *Rnf212b* gene

showed some complexity: two 5' UTR variants were identified in the NCBI database, *variants a* and *b*, which differ by a deletion of the second untranslated exon in *variant b*. By RT-PCR, both variants were expressed in kidney, but neither was expressed in testes (**Figures S1B** and **S1C**). A third *variant c*, that is expressed in testes, was identified by 5' RACE and comprises ~1/3 of the third untranslated exon of *variant a* followed by the 14 coding exons (**Figure 1B**, and **Figures S1B** and **S1C**)**.** In addition, four different coding isoforms were identified in the NCBI database. Isoform a encodes the full-length RNF212B protein of 297 amino acids; isoform b uses an alternative splice acceptor site, creating a premature stop codon after exon 10 that is predicted to produce a protein lacking 86 C-terminal amino acids; isoform c uses an alternative splice donor site to precisely skip exon 10, which corresponds to 16 amino acids of the disordered serine-rich C-terminal tail, resulting in a predicted protein of 270 amino acids; and isoform d lacks the first two exons present in other isoforms and uses an extended exon 3 and most of exon 4 as a 5' UTR, to encode a predicted protein of 189 amino acids that lacks the N-terminal RING finger domain. By RT-PCR, isoforms a, c and d were expressed in both kidney and testis, while isoform b appeared to be testis specific. Expression of full-length a and b isoforms in testis was confirmed by *de novo* cloning from testis mRNA (the sequence of cloned isoform b was similar

but not identical to XR_874633; **Figures S1B** and **S1C**).

Rnf212b$^{-/-}$ mutant mice are sterile due to diminished crossing over

Null mutants in *Rnf212b* were created by pronuclear injection with CRISPR-Cas9, targeting sequences immediately downstream of the first ATG (**Figure 1B)**. Seven mutated lines were obtained, the mutations and phenotypes of which are summarized in **Table S1**. Two identical mutant lines, with a single nucleotide insertion that results in a frameshift after the eighth codon and a premature stop codon after just 27 codons, were chosen for detailed phenotypic analysis (**Figure 1B**).

Heterozygous mutant animals were backcrossed four times and then bred to homozygosity. Mature *Rnf212b*$^{-/-}$ mutant males had testes that were ~3-fold smaller than their wild-type counterparts (means ± SDs of 219.8 ± 16.8 mg per pair of testes from 8 wild-type mice versus 71.6 ± 7.8 mg from 6 *Rnf212b*$^{-/-}$ mice; $p < 0.0001$, two-tailed *t* test; **Figure 1C**), the cauda epididymides were devoid of sperm and the animals were sterile. Testis sections from *Rnf212b*$^{-/-}$ mutant males revealed the presence of metaphase-I spermatocytes, but post-metaphase-I

stages and spermatozoa were absent indicating loss of spermatocytes at stage XII (**Figure 1D**). Female *Rnf212b*$^{-/-}$ mutants were also sterile, but ovaries of 18 days postpartum (dpp) mice contained large numbers of oocytes (**Figures 1E** and **1F**).

Rnf212$^{-/-}$ mutants are sterile because crossing over almost completely fails, producing unconnected univalent chromosomes at metaphase I [21]. To determine whether this is also the case for *Rnf212b*$^{-/-}$ mutants, chromosome spreads from diakinesis/metaphase-I spermatocytes and metaphase-I oocytes were analyzed (**Figure 1G**). In wild-type nuclei, all autosomes presented as bivalents with 24.1 ± 2.3 and 24.6 ± 2.4 chiasmata in spermatocytes and oocytes, respectively (means ± SDs; *n* = 61 spermatocytes and 38 oocytes). Conversely, *Rnf212b*$^{-/-}$ cells contained primarily univalents with a residual of 1-3 chiasmata per nucleus (means ± SDs; 0.66 ± 0.75 and 1.11 ± 0.92 chiasmata from 77 spermatocytes and 28 oocytes, respectively). Surface-spread pachytene-stage chromosomes revealed that *Rnf212b*$^{-/-}$ mutant meiocytes completely failed to form crossover-specific MLH1 foci (**Figure 1H**), indicating defects in the maturation of crossover-specific recombination complexes. This inference was confirmed by analyzing three other crossover-specific markers, HEI10, PRR19 and CDK2 (**Figure S2**)[22,43,44].

To begin to understand the defects in the *Rnf212b*$^{-/-}$ mutant that cause crossover failure, progression through meiotic prophase-I was assessed by quantifying the fractions of spermatocytes at each substage (leptonema, zygonema, pachynema and diplonema; **Figures S3A** and **S3B**). Stage distributions indicated a significant overrepresentation of zygotene-stage spermatocytes in *Rnf212b*$^{-/-}$ mutant spermatocytes and fewer cells in pachytene relative to wild type (p = 0.001, G test) suggesting delayed or unstable synapsis. Consistently, X-Y chromosomes were frequently unsynapsed in pachytene-stage *Rnf212b*$^{-/-}$ mutant spermatocytes, although they were always in close proximity (**Figures S3C** and **S3D**). Unsynapsed X-Y chromosomes were over 5-fold more frequent in the *Rnf212b*$^{-/-}$ spermatocytes relative to wild type (28.6%, n = 57/199 cells from 3 mice and 5.7%, n = 9/158 cells from 3 mice, respectively; p < 0.0001, Fisher's exact test) and were observed specifically in mid/late pachytene cells (staining positive for the histone variant H1t) indicating premature X-Y de-synapsis analogous to that seen in the *Rnf212*$^{-/-}$ mutants [21].

Intermediate steps of meiotic recombination are defective in *Rnf212b*$^{-/-}$ mutants

The modest synapsis defects of the *Rnf212b*$^{-/-}$ mutant suggest that early steps of recombination are generally normal, with RNF212B promoting later steps of crossover differentiation and/or maturation. To test these inferences, a variety of recombination markers were analyzed by immunostaining surface-spread spermatocyte chromosomes (**Figures 2**, **S4** and **S5**). RAD51 and DMC1 assemble onto resected DSB ends to form nucleoprotein filaments that catalyze homologous pairing and DNA strand exchange [12]. The numbers of RAD51 and DMC1 foci detected in zygotene spermatocytes were slightly elevated in the *Rnf212b*$^{-/-}$ mutant relative to wild type (**Figure S4**), suggesting a mild perturbation of recombination as chromosomes synapse that might reflect the delayed/unstable synapsis inferred above (**Figure S3**).

Replication protein A (RPA; comprising RPA1, RPA2 and RPA3) binds single-stranded DNA formed at DSB ends and at D-loops as strand exchange ensues [45]. Prominent immunostaining foci of RPA2 emerge in zygonema, as DMC1 and RAD51 foci are diminishing, and then disappear as DSB repair ensues during pachynema. In mid-zygonema, *Rnf212b*$^{-/-}$ and wild-type spermatocytes formed similar numbers of RPA2 foci, but in subsequent stages levels were significantly lower in *Rnf212b*$^{-/-}$ cells suggesting that DSBs are repaired faster in the mutant

(**Figures 2A** and **2B**). More dramatic reductions were observed for the ZMM proteins MSH4, TEX11^{Zip4} and HFM1^{Mer3}, with ~3-fold fewer foci in the *Rnf212b*$^{-/-}$ mutant (**Figures 2C**, **2D** and **S5**). The altered dynamics of RPA2 and ZMM factors in *Rnf212b*$^{-/-}$ mutant spermatocytes were similar to those seen for *Rnf212*$^{-/-}$, although reduction of MSH4 foci appears to be more severe in *Rnf212b*$^{-/-}$ cells (**Figures 2** and **S5**; Reynolds et al., 2013)

RNF212B dynamically localizes to synaptonemal complexes and recombination sites

To address the possibility that RNF212B functions locally at prospective crossover sites, antibodies were raised against full-length RNF212B (isoform a) and used to immunostain surface-spread spermatocyte chromosomes (**Figures 3A**, **3B** and **S6**). RNF212B was first detected in very early zygonema, specifically localizing to sites of synapsis initiation marked by SYCP1 (73.1% of short SYCP1 stretches <2 μm colocalized with RNF212B foci; 38/52, 11 nuclei). As synapsis ensued, a punctate staining pattern emerged along extending SCs, with focus numbers peaking in early pachynema at 175.9 ± 15.2 foci per nucleus (mean ± SD; 27 nuclei; **Figure 3B**). Focus numbers then reduced throughout pachynema, but at the same time a small number of large, bright RNF212B foci emerged. By late pachynema, each SC had only one

or two large RNF212B foci with 25.0 ± 2.3 foci per nucleus (mean ± SD; 29 nuclei; **Figure 3B**). By mid-diplonema, as homologs desynapsed, all RNF212B foci had disappeared.

Super-resolution structured illumination microscopy (SIM) revealed that RNF212B, like RNF212, localizes specifically to the central region of the SC (**Figure 3C**).

When analyzed by structured illumination microscopy (SIM), a 2-fold excess of RNF212B foci relative to foci of the ZMM factor MSH4 was detected during early pachynema, just after synapsis was complete (**Figures 3D** and **3E**; 290.0 ± 38.3 and 149.4 ± 17.8 foci per nucleus, respectively; means ± SDs; 7 nuclei). Reflecting this excess, only 40.2 ± 6.2 % of RNF212B foci colocalized with recombination sites marked by MSH4 foci; however, 77.2 ± 4.7% MSH4 foci colocalized with RNF212B (means ± SDs; 7 nuclei; **Figures 3D** and **3E**). In late pachynema, numbers of RNF212B foci were indistinguishable from those of the crossover marker MLH1 and colocalization was essentially absolute (**Figure 3F**; 99.7 ± 1.0 % of RNF212B foci colocalized with MLH1 foci and 99.0 ± 1.7 % of MLH1 foci colocalized with RNF212B foci; means ± SDs; 15 nuclei). Thus, RNF212B specifically localizes to crossover sites in late-pachytene spermatocytes.

Chromosomal localization of RNF212B is sexually dimorphic

In fetal oocytes, the initial staining pattern of RNF212B during zygonema was very similar to that observed in spermatocytes, with specific localization to regions of homolog synapsis (**Figures 3I** and **S7**). Focus numbers peaked in early pachynema (defined as pachytene-stage oocytes with ≤3 MLH1 foci from embryonic day E16.5) at 279.0 ± 50.4 foci per nucleus (mean ± SD; 11 nuclei; **Figure 3I**), much higher than the 175.9 ± 15.2 foci per nucleus seen in early pachytene spermatocytes. Also distinct from spermatocytes, high numbers of RNF212B foci persisted along SCs throughout pachynema as large crossover-specific foci emerged at prospective crossover sites. Even after crossover sites had matured, in pachytene oocytes with ≥20 MLH1 foci, RNF212B foci averaged 229.5 ± 45.0 per nucleus (from E18.5 ovaries; mean ± SD; 22 nuclei; **Figures 3G** and **3I**). Moreover, RNF212B remained on synapsed regions throughout diplonema as homologs desynapsed and disappeared only as oocytes entered the dictyate stage (**Figures 3H**, **3I** and **S7**).

RNF212B colocalizes with RNF212 but shows stronger and earlier accumulation at

prospective crossover sites

The phenotypes of *Rnf212b*$^{-/-}$ mutants and the localization dynamics of the RNF212B protein indicate strong similarities with RNF212. To explore the relationship between RNF212B and RNF212, colocalization was analyzed using SIM. In late zygotene/early pachytene stage spermatocytes, when focus numbers peaked, an average of 307.5 ± 50.0 RNF212B foci were detected per nucleus compared to 374.6 ± 43.2 RNF212 foci, and 233.4 ± 38.7 RNF212B-RNF212 co-foci. Thus colocalization level is high but incomplete, with 75.9 ± 3.4% of RNF212B foci colocalized with RNF212, whereas 62.1 ± 5.1% of RNF212 foci colocalized with RNF212B (means ± SDs; 11 nuclei; **Figures 4A** and **4C**).

As pachytene progressed, one or two larger foci of RNF212B and RNF212 emerged along each SC and were both clearly differentiated into crossover foci by late pachynema. To quantify the degree and timing of the differentiation of these large crossover-specific foci, crossover sites were first defined by the presence of the ubiquitin ligase, HEI10, which emerges as crossover-specific immunostaining foci by mid pachynema, significantly earlier than MLH1 (**Figures S8A** and **S8B**), and coincident with the emergence of bright RNF212B foci (**Figure S9**).

The intensity of each RNF212B or RNF212 focus was then measured from images with matched exposures and normalized to the mean intensities of foci in early pachytene nuclei in which HEI10 foci were not yet detected (2,449 RNF212B foci and 2,513 RNF212 foci; 8 nuclei; **Figure 4B**, **4D** and **S8C**).

In mid-pachytene nuclei that had at least one clear HEI10 crossover focus on each autosomal SC (i.e. ≥19 HEI10 foci per nucleus), the RNF212B foci located at crossover sites (i.e. colocalizing with HEI10 foci) were 11-fold brighter than other RNF212B foci in the same nuclei (i.e. the average of all other foci from the same 8 nuclei; 6.29 ± 2.66 for 194 crossover foci versus 0.57 ± 0.59 for 2,004 other foci from 8 nuclei; means ± SDs; $p < 0.0001$, Mann-Whitney test) and 6.3-fold brighter than the foci detected in early pachytene nuclei. The same analysis showed that RNF212 foci located at crossover sites were only 3-fold brighter than other foci in the same nuclei (1.83 ± 1.05 for 194 crossover foci versus 0.60 ± 0.58 for 2,291 other foci form 8 nuclei; means ± SDs; $p < 0.0001$, Mann-Whitney test) and 1.8-fold brighter than those in early pachytene. Thus, at designated crossover sites in mid pachytene, RNF212B foci show stronger differentiation than RNF212 foci.

In late pachytene spermatocytes, the only remaining RNF212B foci were crossover specific and had intensities comparable to those of the crossover foci analyzed in mid-pachytene nuclei (6.42 ± 4.84-fold brighter than early pachytene foci; 206 crossover foci from 8 nuclei; mean ± SD) suggesting that RNF212B foci do not continue to enlarge between mid and late pachytene. RNF212 staining in late pachytene nuclei comprised a mixture of crossover foci and other small residual foci. The crossover-specific RNF212 foci in these nuclei were 6-fold brighter than other foci in the same nuclei (1.53 ± 1.13 for 206 crossover foci versus 0.24 ± 0.23 for 988 other foci from 8 nuclei; means ± SDs; $p < 0.0001$, Mann-Whitney test) but only 1.5-fold brighter than those in early pachytene. Thus, crossover-specific RNF212 foci continue to differentiate between mid and late pachynema but this may occur primarily via loss of RNF212 from noncrossover foci as opposed to continued growth of crossover-specific foci.

Per chromosome analysis for mid-pachytene autosomes highlighted additional distinctions between RNF212B and RNF212 with respect to the differentiation of larger crossover-correlated foci (**Figures 4E** and **S8D**). RNF212B foci at crossover sites were on average 5.1-fold brighter

relative to the brightest other focus along the same chromosome, whereas RNF212 foci were only 1.4-fold brighter (**Figure 4E**, left). When these relative intensities were plotted for individual pairs of colocalizing RNF212-RNF212B crossover foci, almost no correlation was detected (r^2 = 0.106) indicating that high intensity RNF212B foci are not coincident with high intensity RNF212 foci during mid pachytene; and pointing to distinct differentiation behaviors of the two proteins at crossover sites (**Figure 4E**, right).

In mid-pachynema, 76.1% of crossover sites (140/184; 8 nuclei) showed strong differentiation for RNF212B foci (≥2-fold brighter relative to the brightest other focus along the same chromosome) but not for RNF212 foci. Oppositely only 0.5% of crossover sites (1/184; 8 nuclei) showed strong differentiation of only RNF212 but not RNF212B (**Figure 4E**, right). Together, these data imply that crossover-specific patterning of RNF212B occurs earlier than that of RNF212. The distinct behaviors of RNF212B and RNF212 were most pronounced in nuclei transitioning between early and mid-pachynema, as bright HEI10 foci were emerging (i.e. nuclei with <19 HEI10 foci per nucleus; **Figure 4F**). In these nuclei, RNF212B showed clear differentiation at prospective crossover sites but RNF212 did not. Together, our data are consistent with crossover foci of

RNF212B differentiating during early-to-mid pachytene primarily via growth (i.e. accumulation of RNF212B), while RNF212 crossover foci differentiate during mid-to-late pachytene and loss of RNF212 from other sites may make a more significant contribution to changes in relative intensity.

In females, as noted above, both RNF212B and RNF212 retain significant general staining along SCs throughout pachynema (**Figures 3G, 3I** and **S7**). Nonetheless, the differentiation of RNF212B at crossover sites was also more pronounced than that of RNF212, indicating that the distinct dynamics of the two proteins is a common feature of male and female meiosis (**Figure S8E**).

Similar but distinct behaviors of RNF212B and RNF212 in mutants defective for recombination and synapsis

The relationship between RNF212B and RNF212 was further explored by analyzing their localizations in mutants defective for recombination or synapsis. Repair of SPO11-induced DSBs by recombination is required for the alignment and synapsis of homologs. Thus, *Spo11*$^{-/-}$ mutant

meiocytes are defective for synapsis, although extensive stretches of SC between non-homologous axes are observed in some nuclei [46,47]. In *Spo11*$^{-/-}$ spermatocytes, RNF212B staining was still detected specifically on synapsed regions marked by SYCP1, as previously seen for RNF212 (**Figure 5A**)[21]. Intensities of RNF212B immunofluorescence along synapsed regions in *Spo11*$^{-/-}$ nuclei with late zygotene/early pachytene-like morphologies (well-developed SYCP3-staining axes and extensive synapsis, albeit non-homologous) were ~50% lower than those in equivalent early-pachytene *Spo11*$^{+/+}$ nuclei (**Figure 5B**). By contrast, intensities of SC-associated RNF212 immunostaining were comparable for *Spo11*$^{-/-}$ and *Spo11*$^{+/+}$ nuclei. Correspondingly, the normalized ratio of RNF212B / RNF212 immunofluorescence intensity on synapsed regions was reduced by ~50% in *Spo11*$^{-/-}$ spermatocytes (**Figure 5B**). Thus, Spo11-initiated recombination differentially influences the association of RNF212B and RNF212 with synaptonemal complexes, with only RNF212B showing a significant dependence.

SYCP1 is the major component of the SC central element. Although *Sycp1*$^{-/-}$ mutant meiocytes fail to assemble SCs, recombination initiates normally, and homolog axes become coaligned [48]. In *Sycp1*$^{-/-}$ spermatocytes, RNF212B staining was barely detectable in early/mid zygotene-like

nuclei indicating that initial association with meiotic chromosomes is strongly dependent on the SC central region (**Figure S10A**). However, relatively dim RNF212B foci could be detected between aligned homologous axes in late zygotene/early pachytene-like nuclei that had extensive homolog coalignment (**Figures 5C**). The majority of these RNF212B foci localized to recombination sites, revealed by a high level of colocalization with RPA2 (71.0 ± 8.0%; mean ± S.D., 8 nuclei), as seen previously for RNF212 localization in *Sycp1*$^{-/-}$ spermatocytes (**Figures 5C** and **S10B**)[21]. Thus, normal localization of RNF212B to prophase-I chromosomes is strongly dependent on synapsis, with respect to both timing and abundance, but RNF212B can independently localize to recombination sites, albeit inefficiently.

RNF212B focus numbers in *Sycp1*$^{-/-}$ nuclei were reduced 2.4-fold relative to *Sycp1*$^{+/+}$ controls (192.1 ± 18.3 foci in *Sycp1*$^{+/+}$ versus 81.4 ± 19.3 in *Sycp1*$^{-/-}$; mean ± SDs; **Figure 5D**). Correspondingly, the degree of RPA2 colocalization with RNF212B was reduced 2.4-fold (from 67.3 ± 3.7% in *Sycp1*$^{+/+}$ to 27.9 ± 6.0% in *Sycp1*$^{-/-}$; means ± S.D.; n = 7 and 8 nuclei, respectively; p = 0.0002, Mann-Whitney test) and RNF212B-RPA2 co-foci were reduced 1.9-fold (109.4 ± 7.4 foci in *Sycp1*$^{+/+}$ versus 57.9 ± 14.7 in *Sycp1*$^{-/-}$; mean ± SDs; **Figures 5E** and **S10C**)

In contrast, in the same nuclei, numbers of RNF212-RPA2 co-foci remained essentially unchanged (122.4 ± 7.8 foci in *Sycp1*$^{+/+}$ versus 131.3 ± 17.4 in *Sycp1*$^{-/-}$; mean ± SDs) despite a 1.5-fold reduction in total RNF212 focus numbers (220.3 ± 13.9 foci in *Sycp1*$^{+/+}$ versus 146.9 ± 21.4 in *Sycp1*$^{-/-}$; mean ± SDs; **Figures 5D** and **S10C**). Moreover, the degree of RPA2-RNF212 colocalization was barely altered (75.2 ± 2.9% in *Sycp1*$^{+/+}$ versus 64.3 ± 11.6% in *Sycp1*$^{-/-}$; mean ± SDs; $p = 0.0578$, Mann-Whitney test; **Figure 5E**).

We infer that the localization of RNF212B to recombination sites shows a greater dependence on synapsis than does RNF212. Consequently, this differential dependency resulted in reduced colocalization of RNF212B and RNF212 foci in *Sycp1*$^{-/-}$ spermatocytes (61.8 ± 9.0% of RNF212B foci colocalized with RNF212, and 33.9 ± 6.3% of RNF212 foci colocalized with RNF212B; versus 95.8 ± 2.4% and 83.8 ± 8.6% in wild-type *Sycp1*$^{+/+}$ nuclei; mean ± SDs; **Figure S10D**).

MLH3 and MLH1 constitute the MutLγ complex that facilitates the crossover-specific resolution of double-Holliday junctions [15,16]. Consistently, *Mlh3*$^{-/-}$ meiocytes are proficient for synapsis and

early steps of meiotic recombination, but severely defective for crossover formation [49]. RNF212B staining in *Mlh3*$^{-/-}$ spermatocytes was comparable to *Mlh3*$^{+/+}$ controls: focus numbers peaked in early pachynema, then diminished as pachynema progressed with one or two large RNF212B foci emerging on each SC (**Figures 5F**, **5G**, **S10E** and **S10F**). Thus, the differentiation of RNF212B into crossover-specific foci precedes crossover formation and does not require the crossover-specific factor, MutLγ. Numbers of large crossover-specific RNF212B foci in late pachytene *Mlh3*$^{-/-}$ nuclei were slightly lower than in wild-type *Mlh3*$^{+/+}$ controls, possibly reflecting reduced stability or altered efficiency of formation (**Figure S10F**). In addition, unlike wild type, some smaller foci remained on the SCs until late pachynema in *Mlh3*$^{-/-}$ nuclei suggesting some additional signal following the maturation of crossover sites may trigger the complete loss of RNF212B from noncrossover sites.

RNF212 staining in *Mlh3*$^{-/-}$ mutant spermatocytes was comparable to wild-type cells in early pachynema, but the differentiation of crossover-specific foci was not as conspicuous; and overall focus numbers remained relatively high throughout pachynema (**Figures 5F**, **5G**, and **S10F**). Moreover, numerous RNF212 foci persisted on synapsed regions in early diplotene *Mlh3*$^{-/-}$ nuclei

in which RNF212B staining was barely detectable. Together, analysis of RNF212B and RNF212 localization in mutant contexts extends our inference that the localization dynamics and regulation of these two crossover factors is distinct.

HEI10 is required for crossover-specific patterning of RNF212B

Our previous studies evoked a model in which RNF212 establishes a precondition for crossover/noncrossover differentiation by stabilizing nascent recombination intermediates and rendering further progression of meiotic recombination dependent on HEI10 [22,23]. In *Hei10*$^{mei4/mei4}$ mutant meiocytes, abundant RNF212 foci persist along synapsed chromosomes and recombination stalls at an intermediate step marked by the persistence of ZMM foci throughout pachytene [22,23]. Similarly, RNF212B staining in early pachynema *Hei10*$^{mei4/mei4}$ mutant spermatocytes was indistinguishable from wild type, but this pattern of abundant foci along SCs persisted until early diplonema (**Figures S11A** and **S11B**). Moreover, in sharp contrast to the complete differentiation of RNF212B into crossover-specific foci seen in wild-type late-pachytene nuclei (24.8 ± 2.7 foci, mean ± SD from 16 nuclei), a majority of chromosomes in *Hei10*$^{mei4/mei4}$ mutant nuclei had no detectable differentiation of RNF212B foci (**Figures S11C** and **S11D**).

Specifically, for 54.4% of individual chromosomes from late pachytene *Hei10*$^{mei4/mei4}$ spermatocyte nuclei (with strong H1t staining), neither the first nor the second brightest focus was ≥1.5-fold brighter than the third brightest focus along the same chromosome, and only 17.0 % of individual chromosomes had RNF212B foci that were ≥2-fold brighter than the third brightest focus along the same chromosome (93/171 and 29/171 chromosomes, respectively; 9 nuclei; **Figures S11A** and **S11C**). The most differentiated RNF212B foci were on average 1.6-fold brighter, with a maximum of 4.2-fold, relative to the third brightest focus along the same chromosome in late pachytene *Hei10*$^{mei4/mei4}$ spermatocyte nuclei; whereas in wild-type mid-pachytene nuclei, RNF212B foci at crossover sites were on average 6.7-fold brighter relative to the brightest other focus along the same chromosome (**Figures S11D**; wild-type chromosomes with two crossover foci were used for comparison to *Hei10*$^{mei4/mei4}$ chromosomes). Thus, differentiation of RNF212B into crossover-specific foci is largely dependent on HEI10.

RNF212B and RNF212 are interdependent for chromosomal localization and protein stability

Our localization analysis argues against the idea that RNF212B and RNF212 function as an

obligate heterocomplex of fixed stoichiometry. Even so, immunostaining analysis in *Rnf212b*$^{-/-}$ and *Rnf212*$^{-/-}$ mutants indicated an interdependent relationship. RNF212 immunostaining was diminished in *Rnf212b*$^{-/-}$ mutant meiocytes and, likewise, RNF212B immunostaining was diminished in *Rnf212*$^{-/-}$ cells (**Figures 6A** and **6B**). Immunoblotting for RNF212 and RNF212B revealed that protein levels were greatly reduced in testis extracts from *Rnf212b*$^{-/-}$ and *Rnf212*$^{-/-}$ mutants, respectively, relative to wild-type controls (**Figure 6C**; in these experiments, RNF212B was first immunoprecipitated because it was not readily detectable in whole-cell extracts).

Interaction between RNF212B and RNF212 was detected by yeast two-hybrid assay, and self-interaction for both proteins was also observed (**Figure 6D**). These results indicate that RNF212B and RNF212 are mutually dependent for protein stability and thus chromosomal localization, and that they can physically interact.

The RING finger domain of RNF212B is required for self-interaction and function *in vivo*

RNF212B and RNF212 are both putative SUMO E3 ligases with N-terminal RING finger domains. Mutation of conserved zinc-coordinating cysteine or histidine residues within RING finger

domains typically ablates ligase activity, and can disrupt interaction with partner proteins, as seen for the obligate ligase heterodimer [50]. Our analysis argues against the idea that RNF212B and RNF212 function exclusively as an obligate heterodimer (or high order oligomer with fixed stoichiometry), but their functional interdependence and physical interaction led us to explore the role of the RING domain. Yeast two-hybrid analysis revealed that mutation of cysteine 9 of the RNF212B RING finger domain (RNF212B^{C9A}) did not affect RNF212-RNF212B interaction but disrupted self-interaction of RNF212B (**Figure 6E**). However, the analogous mutation in RNF212 (RNF212^{C10A}) did disrupt RNF212-RNF212B interaction. Additional insight into role of the RNF212B RING finger domain was obtained by analyzing a *Rnf212b* RING mutant mouse line carrying a deletion of the three nucleotides that encode cysteine 9 (**Figure S12**). Homozygous mutant mice (hereafter referred to as *Rnf212b*$^{RING/RING}$) were sterile, mature males had smaller testes and cauda epididymides were devoid of sperm (comparable to the *Rnf212b*$^{-/-}$ null mutant). Chromosome spreads from diakinesis/metaphase-I spermatocytes and metaphase-I oocytes revealed primarily univalent chromosomes with residual levels of chiasmata that were indistinguishable from those seen in *Rnf212b*$^{-/-}$ null mutant mice. Detailed analysis of *Rnf212b*$^{RING/RING}$ mutant spermatocytes revealed nearly identical phenotypes to those of the

Rnf212b$^{-/-}$ mutant: absence of MLH1 foci, elevated frequencies of prematurely desynapsed X-Y chromosomes and reduced numbers of RPA2 and ZMM foci (**Figure S12**).

Immunoblotting of *Rnf212b*$^{RING/RING}$ testis extracts revealed diminished levels of both RNF212B and RNF212, comparable to those seen in extracts from *Rnf212b*$^{-/-}$ mutant testes (**Figure 6F**). Consequently, chromosomal localization of both RNF212B and RNF212 was diminished in *Rnf212b*$^{RING/RING}$ mutant meiocytes (**Figures 6G** and **6H**). Thus, an intact RING finger domain in RNF212B is essential for the stability of both RNF212B and RNF212 proteins *in vivo*.

DISCUSSION

Global and local regulation of recombination by RNF212B, RNF212, and HEI10

RNF212B is the third Zip3-like protein identified in mammals that functions at recombination sites to promote crossing over. Like its paralog, RNF212, RNF212B initially localizes as numerous foci along the SC central region; and then repatterns to localize specifically at prospective crossover sites, while diminishing elsewhere. A key question for understanding meiotic crossover control is whether the repatterning of Zip3-like proteins along SCs is responsible for specifying crossover

sites, as proposed by models that invoke phase-transition, coarsening, and/or condensation processes [25,51-53]; or whether it is a downstream consequence of crossover patterning via a distinct process such as the mechanical stress envisioned in the beam-film model [54 55]. The latter possibility does not necessarily exclude coarsening behavior of Zip3-like proteins, which could have other functions. Among the three mammalian Zip3-like proteins, only RNF212B shows dynamics that could be compatible with a role in mediating crossover patterning and indicates that this process occurs no later than early pachytene. By contrast, the differentiation of RNF212 foci appears to be a later event; and HEI10 does not perceptively localize along SCs before appearing at crossover sites (with the caveat that undetectable levels HEI10 could be involved).

Notwithstanding potential roles in crossover patterning, what might be the function(s) of the observed dynamics of RNF212, RNF212B and HEI10? Our analysis emphasizes the interdependencies and distinctions between RNF212, RNF212B and HEI10, and their global and local functions that help coordinate key events of meiotic prophase I. Most evident is regulating the progression of recombination occurring in the context of the SC. Following initial DNA strand-exchange and homolog pairing, RNF212-RNF212B associates with nascent SCs and

acts to stabilize ZMM factors and pause the progression of recombination. In this way, RNF212-RNF212B may act to protect nascent recombination intermediates from being prematurely dissociated by the Bloom complex, which is inferred to mediate the default noncrossover outcome of recombination via synthesis-dependent strand annealing [14,35-37,56]. This early function of RNF212-RNF212B appears to promote and stabilize synapsis, possibly acting as a kind of proofreading mechanism that selectively reinforces SC assembled at recombination sites, i.e. between homologous chromosomes. As prophase-I progresses, connection of homologs by recombinational interactions is superseded by the SC. RNF212-RNF212B could mediate this hand-off by ensuring that recombinational connections are not lost until mature SC has formed.

Pausing the progression of SC-associated recombination events may also be a prerequisite for crossover/noncrossover differentiation and/or allow time for crossover sites to mature. Importantly, RNF212-RNF212B renders the progression of recombination dependent on HEI10 (**Figure S11**) and additional pro-crossover factors including kinase CDK2, and the CNTD1-PRR19 complex [22,23,43,57,58]. In the absence of HEI10, foci of RNF212-RNF212B and

ZMM proteins remain abundant and undifferentiated along SCs, and recombination continues to be stalled throughout pachytene, with DSB repair being completed only as the SC central region disassembles along with RNF212-RNF212B.

At designated crossover sites, local protection of intermediates via RNF212-RNF212B may continue to impede noncrossover resolution mediated by the Bloom complex, and thereby enable crossover-specific events including dHJ formation and recruitment of the crossover-specific resolution machinery, organized around the MutLγ endonuclease. Local stabilization of SC via RNF212-RNF212B may also explain why crossover sites are the last sites to desynapse during diplotene [59]. We have suggested that patches of SC retained at crossover sites may help coordinate the DNA events of crossing over with exchange of the underlying chromosome axes to form chiasmata.

Distinct and interdependent functions of RNF212, RNF212B and HEI10

Our ability to discern potentially distinct functions of RNF212 and RNF212B is compromised by their interdependence for protein stability, i.e. *Rnf212* and *Rnf212b* single mutant phenotypes

likely reflect diminished function of both proteins. However, our analysis of the localization dynamics of RNF212 and RNF212B revealed divergent behaviors of the two proteins that point to distinct function and regulation.

For example, in early pachytene nuclei, RNF212 foci outnumber RNF212B and up to 40% don't colocalize. Also, the differentiation of crossover specific RNF212B foci was much stronger than for RNF212 and occurred earlier, with the suggestion that differentiation may occur via distinct processes, e.g. redistribution to crossover sites for RNF212B, versus the loss from noncrossover sites for RNF212 (or via different proportions of redistribution and loss). Thus, although RNF212 and RNF212B interact, these observations argue against the existence of an obligate heterocomplex of fixed stoichiometry and suggest that the activity of RNF212B may be modulated by switching binding partners as it accumulates at prospective crossover sites. For example, RNF212B-RNF212B self-interaction could become prominent at prospective crossover sites; or RNF212B could partner with HEI10 in order to locally accumulate and modulate E3 ligase activities at designated crossover sites. Consistent with the latter possibility, the differentiation of RNF212B foci is both dependent on HEI10 and temporally indistinguishable

from its appearance at prospective crossover sites (**Figures S9** and **S11**).

Localization dynamics in mutant backgrounds also point to distinct functions and regulation of RNF212, RNF212B and HEI10. For example, RNF212 localization along SCs remains robust in the absence of SPO11-catalyzed DSBs while localization of RNF212B is much less efficient, suggesting that DSB signaling may stabilize RNF212B. In this respect, RNF212B may be like budding yeast Zip3, which requires phosphorylation at S/T-Q consensus sites for the DNA-damage response (DDR) kinases $Mec1^{ATR}$/$Tel1^{ATM}$ for normal localization [60]. Further distinctions are seen in the absence of synapsis, with RNF212 showing a robust ability to localize to recombination sites, while RNF212B localization was much weaker. Thus, inputs from both DSBs and synapsis appear to stabilize RNF212B and thereby coordinate its activity in space and time, while RNF212 might act more as an anchor for localization to SCs and recombination sites. We previously showed that HEI10 foci are largely dependent on both DSBs and synapsis [22], consistent with our inference that HEI10 foci assemble only as crossover sites differentiate, dependent on RNF212-RNF212B.

Defective crossover maturation in the *Mlh3* mutant impacts the dynamics of RNF212, RNF212B and HEI10 to varying degrees. Although crossover-specific RNF212-RNF212B foci are clearly differentiated in *Mlh3* spermatocytes, small foci of RNF212, and to a lesser extent RNF212B, also persist along SCs implying that a signal associated with the maturation of crossover sites enhances the general loss of RNF212-RNF212B from noncrossover sites. We previously showed that HEI10 patterning is severely perturbed in *Mlh3* mutant spermatocytes, with abnormally high numbers of foci (~90 per nucleus) forming earlier than normal and then persisting at recombination sites until chromosomes desynapse [22]. Thus, although HEI10 is required for crossover patterning of RNF212-RNF212B foci, this function does not necessarily require crossover-specific patterning of HEI10 itself, i.e. crossover-specific localization of HEI10 appears to be downstream of initial crossover patterning and requires a maturation step that is dependent on MLH3.

Collectively, these data suggest that RNF212, RNF212B and HEI10 may function as apical effectors that coordinate meiotic prophase by integrating signals from synapsis, DSB repair, cell cycle kinases, and maturating crossover sites (**Figure 7**).

Sexual dimorphism

The patterning of RNF212B along SCs shows sexual dimorphism, with complete differentiation in spermatocytes resulting in only large crossover-specific foci; while in oocytes, numerous smaller foci persist throughout pachytene even after larger crossover-specific foci have formed and crossover sites have matured (marked by the appearance of MLH1 foci; **Figures 3G**, **3H** and **S8E**). RNF212 dynamics are similarly dimorphic. These data indicate that complete differentiation of RNF212B is not a prerequisite for the patterning and maturation of crossover sites. Possibly, accumulation of a threshold level of RNF212B at a given recombination site is sufficient for it to mature into a crossover. However, incomplete differentiation could render RNF212B crossover foci less stable and potentially reversible in females, possibly accounting for the inefficiency of crossover maturation characterized in human oocytes that can result in unconnected (achiasmate) homologs, or homologs connected only by a single telomere-proximal chiasma, configurations that are prone to segregation error [8,9].

What could account for the sexually dimorphic behavior of RNF212B? A pertinent difference may

be the duration of pachytene, which lasts almost 7 days in mouse spermatocytes [61] compared to just 1-2 days in oocytes [62]. Thus, if RNF212B repatterning dynamics are relatively slow, differentiation may remain incomplete in oocytes. Also, oocytes SCs are longer than males and RNF212B appear to be generally more abundant, with almost 60% more foci in females.

FIGURE LEGENDS

Figure 1. RNF212B is a RING finger-containing protein required for crossing over and fertility in mouse.

(A) Domain structures of mouse RNF212B and RNF212. Amino acid sequences of the RING finger domains are shown below. Presumptive zinc-coordinating cysteines and histidines and other identical residues are highlighted in pink and blue, respectively.

(B) Schematic of the mouse *Rnf212b* gene on chromosome 14. Top row: red and black bars represent 5' untranslated exons (5' UTRs) and coding exons, respectively. Middle row: yellow and blue boxes represent 5' UTRs and coding exons, respectively, in the full-length isoform a. The inverted red triangle represents the translation initiation site in testis identified by 5' RACE. An asterisk represents the stop codon. Horizontal bars represent the positions of primers used to

detect 5' UTR variants a/b/c by RT-PCR in **Figure S1C**. Bottom row: nucleotide and amino-acid sequences at the CRISPR/Cas9 targeted site in exon 1. A single-nucleotide insertion (shown in red) created a frameshift and premature stop codon (asterisk). The guide RNA (gRNA) sequence is highlighted in blue.

(C) Reduced testis size in *Rnf212b*$^{-/-}$ mutant males. Red bars indicate means. ****$p \leq 0.0001$ for a two-tailed *t* test. n, numbers of mice analyzed.

(D) Defective spermatogenesis in *Rnf212b*$^{-/-}$ mutant males. Seminiferous tubule sections from wild-type and *Rnf212b*$^{-/-}$ testes stained with hematoxylin and eosin. rSt, round spermatid; eSt, elongated spermatid. Arrowheads indicate metaphase cells.

(E) Ovary sections from wild-type and *Rnf212b*$^{-/-}$ mutant females at 18 days postpartum (dpp) immunostained for p63 and counterstained with hematoxylin.

(F) Oocyte counts at 18 dpp. Red bars indicate means. ns, not significant ($p > 0.05$, two-tailed *t* test). n, numbers of mice analyzed.

(G) Chiasmata are diminished in *Rnf212b*$^{-/-}$ meiocytes. Left panels: diakinesis/metaphase-I stage spermatocytes from wild-type and *Rnf212b*$^{-/-}$ testes stained with DAPI. Right panels, metaphase-I oocytes from ovaries of ≥2-month-old wild-type and *Rnf212b*$^{-/-}$ females stained with

DAPI and immunostained for CREST (centromeres). Scale bars, 10 μm.

(H) MLH1 foci are absent in *Rnf212b*$^{-/-}$ meiocytes. Mid-late pachytene-stage spermatocyte nuclei from wild-type and *Rnf212b*$^{-/-}$ testes (left panels); and pachytene-stage oocyte nuclei from wild-type and *Rnf212b*$^{-/-}$ ovaries at embryonic day 18.5 (right panels) immunostained for SYCP3 and MLH1. Scale bars, 10 μm.

Figure 2. Intermediate steps of recombination are perturbed in *Rnf212b*$^{-/-}$ mutant mice.

(A and C) Wild-type and *Rnf212b*$^{-/-}$ spermatocyte nuclei at the indicated stages immunostained for SYCP3 and RPA2 (A), or SYCP3 and MSH4 (C). Representative chromosomes are magnified in C. Scale bars, 10 μm for full nucleus images and 2 μm for individual chromosomes.

(B and D) Focus counts of RPA2 (B) and MSH4 (D). Red bars indicate means ± SDs. ns, not significant ($p > 0.05$); *$p \leq 0.05$; ***$p \leq 0.001$; ****$p \leq 0.0001$ for two-tailed Mann-Whitney tests. n, numbers of nuclei analyzed.

Figure 3. RNF212B localization to the synaptonemal complexes and recombination sites in prophase I meiocytes.

(A) RNF212B localization in spermatocyte nuclie at successive prophase I stages. Images show surface-spread prophase-I spermatocyte nuclei immunostained for SYCP3, SYCP1, RNF212B and H1t. Arrowheads highlight large RNF212B foci. Arrows indicate synapsed pseudo-autosomal region between the X-Y chromosomes.

(B) Numbers of RNF212B foci per nucleus in spermatocytes at successive prophase I stages. Red bars indicate means. Means of focus numbers are shown below the graph. Lept., leptonema; Zyg., zygonema; pach., pachynema; dip., diplonema. Numbers of nuclei analyzed were 8, 12, 27, 29, 29, 19 and 11 for in leptonema, zygonema, early pachynema, mid pachynema, late pachynema, early diplonema and mid diplonema, respectively.

(C) RNF212B localizes to the central region of the synaptonemal complex. SIM images of early and late pachytene spermatocytes immunostained for SYCP3 and RNF212B. Arrowheads highlight large RNF212B foci.

(D) RNF212B colocalization with MSH4 in early pachynema. SIM images of an early pachytene spermatocyte immunostained for SYCP3, RNF212B and MSH4.

(E) Quantification of RNF212B colocalization with MSH4. Left, focus counts. Right, degree of colocalization. Black and red bars indicate means. 7 early pachytene nuclei were analyzed by

SIM imaging.

(F and G) RNF212B colocalization with MLH1 in spermatocytes (F) and oocytes (G). A late-pachytene spermatocyte (F) and a pachytene oocyte from an embryonic day 18.5 ovary (G) immunostained for SYCP3, RNF212B and MLH1. Arrowheads indicate crossover sites.

(H) Persistent RNF212B staining on synapsed regions in diplotene-stage oocytes. A late diplotene oocyte from a 0.5 days postpartum ovary immunostained for SYCP3 and RNF212B.

(I) Numbers of RNF212B in oocyte nuclei at successive prophase-I stage. Red bars indicate means. Means of focus numbers are indicated below the graph. Numbers of nuclei analyzed in leptonema (at E15.5), zygonema (at E15.5), early pachynema (pachytene nuclei with ≤3 MLH1 foci at E16.5), mid/late pachynema (pachytene nuclei with ≥20 MLH1 foci at E18.5), early diplonema (at 0.5 dpp), mid diplonema (at 0.5 dpp), late diplonema (at 0.5 dpp) and dictyate stage (at 0.5 dpp) are 21, 22, 11, 22, 18, 11, 15 and 7, respectively.

Magnified images in (A), (C), (D), (F), (G) and (H) show representative chromosomes. Scale bars, 10 μm for full nuclei and 2 μm for magnified images.

Figure 4. Similar but distinct localization pattern of RNF212B and RNF212 in

differentiation into crossover foci

(A) RNF212B-RNF212 colocalization. SIM images of a late-zygotene spermatocyte immunostained for SYCP3, RNF212B and RNF212.

(B) Differentiation of RNF212B at prospective crossover sites is stronger than RNF212. Airyscan images of early, mid and late pachytene spermatocytes nuclei immunostained for SYCP3, RNF212B, RNF212 and HEI10. In all cases, RNF212B and RNF212 image exposures are matched. Arrowheads indicate crossover sites marked by HEI10.

(C) Quantification of RNF212B coloclaization with RNF212. Left, focus counts. Right, degree of colocalization. Black and red bars indicate means. 3 late-zygotene and 8 early-pachytene nuclei were analyzed by SIM imaging.

(D) Quantification of focus intensities for RNF212B and RNF212. Bars indicate medians and 25th and 75th percentiles. ****$p \leq 0.0001$ for two-tailed Mann-Whitney tests. 8 nuclei for each stage were analyzed by Airyscan imaging. Total numbers of foci analyzed: 2,449 RNF212B foci and 2,513 RNF212 foci in early pachynema; 194 crossover foci, 2,004 other RNF212B foci and 2,291 other RNF212 foci in mid pachynema; 206 crossover foci and 988 other RNF212 foci. All, all foci; COs, crossover foci colocalized with HEI10 foci; Others, other foci that don't colocalize with

HEI10 foci. ND, not detected. Quantification of focus intensities in representative individual nuclei in (B) is shown in **Figure S8C**.

(E) Per chromosome analysis for autosomes in mid-pachytene spermatocyte nuclei. Intensity of each crossover-associated RNF212B or RNF212 focus relative to that of the next brightest (non-crossover) focus along the same chromosome plotted separately (left) and in two dimensions (right). Red dashed lines indicate a relative focus intensity of 2. Detailed representation of a per chromosome analysis is shown in **Figure S8D**. ****$p \leq 0.0001$ for two-tailed Mann-Whitney tests. 186 crossover foci from 8 mid-pachytene nuclei were analyzed. Two crossover-associated RNF212B foci with no other RNF212B foci along the same chromosome were excluded from the plots.

(F) RNF212B differentiation without detectable RNF212 differentiation during early to mid pachyenema. Airyscan images of an early- to mid-pachytene spermatocyte nucleus, with 8 HEI10 foci, immunostained for SYCP3, RNF212B, RNF212 and HEI10 are shown. Arrowheads indicate crossover sites marked by HEI10. Magnified images in (A), (B) and (F) show representative chromosomes. Scale bars, 10 μm for whole nuclei and 2 μm for magnified images.

Figure 5. Chromosomal localization of RNF212B and RNF212 in mutants defective for recombination and synapsis

(A) RNF212B and RNF212 localize to synapsed regions between non-homologous axes in DSB-defective *Spo11*$^{-/-}$ spermatocytes. Images show a late zygotene/early pachytene-like nucleus immunostained for SYCP3, SYCP1, RNF212B and RNF212.

(B) Staining intensities of RNF212B and RNF212 on synapsed regions. Left, signal intensities per µm of SC per nucleus. Right, ratios of intensities µm of SC for RNF212B relative to RNF212. Black and red bars indicate means. 14 early pachytene *Spo11*$^{+/+}$ nuclei and 10 late zygotene/early pachytene-like *Spo11*$^{-/-}$ nuclei were analyzed.

(C) RNF212B and RNF212 localize to recombination sites between aligned homolog axes in synapsis-defective *Sycp1*$^{-/-}$ spermatocytes. A late zygotene/early pachytene-like nucleus immunostained for SYCP3, RNF212B, RNF212 and RPA2 is shown.

(D and E) Focus counts of RNF212B and RNF212 (D); and degree of RPA2 colocalization with RNF212B and RNF212 (E). Black bars indicate means. 7 early pachytene *Sycp1*$^{+/+}$ nuclei and 8 late zygotene/early pachytene-like *Sycp1*$^{-/-}$ nuclei were analyzed.

(F) Differentiation of crossover-specific RNF212 foci and persistence of RNF212 staining in crossover-defective *Mlh3*$^{-/-}$ spermatocyte nuclei. Late pachytene and early diplotene nuclei immunostained for SYCP3, RNF212B, and RNF212 are shown. Arrowheads indicate large RNF212B foci.

(G) Numbers of RNF212B and RNF212 foci per nucleus in successive late prophase I stages of spermatocytes. Black bars indicate means. Numbers of nuclei analyzed in early pachynema, late pachynema, and early diplonema were 12, 20, and 13 for *Mlh3*$^{+/+}$; and 12, 18, and 13 for *Mlh3*$^{-/-}$. ns, not significant ($p > 0.05$); ***$p \leq 0.001$; ****$p \leq 0.0001$ for two-tailed Mann-Whitney tests. Magnified images in (C) and (F) show representative chromosomes. Scale bars, 10 μm for whole nuclei and 2 μm for magnified images.

Figure 6. Interdependence of RNF212B and RNF212 for chromosomal localization and protein stability and the role of the RING-finger domain.

(A and B) RNF212 (A) and RNF212B (B) are interdependent for chromosomal localization. Early pachytene spermatocyte nuclei (left) and pachytene-stage oocytes at embryonic day 18.5 or 16.5 (E18.5 or E16.5; right) from the indicated genotypes were immunostained for SYCP3 and

RNF212 (A) or RNF212B (B). Scale bars, 10 μm.

(C) Interdependent protein stability of RNF212B and RNF212. Whole-testis extract from indicated genotypes were subjected to immunoblotting for RNF212 and IP-immunoblotting for RNF212B. SYCP3 is a loading control for meiotic cells.

(D) Yeast two-hybrid assay showing interaction between RNF212B and RNF212, and self-interactions for RNF212B and RNF212. Yeast cells expressed the Gal4 activation domain (Gal4-AD) and binding domain (Gal4-BD) fused to the indicated proteins, or empty vectors as controls. Aureobasidin A selection was used to detect reporter activation.

(E) Yeast two-hybrid assay shows that a C9A RING-domain mutation in RNF212B diminishes its self-interaction but not its interaction with RNF212.

(F) Diminished protein levels of RNF212B and RNF212 in *Rnf212b*$^{RING/RING}$ spermatocytes. Whole-testis extract from indicated genotypes were subjected to immunoblotting for RNF212 and IP-immunoblotting for RNF212B. SYCP3 is a loading control of meiotic cells.

(G and H) Chromosomal localization of RNF212B (G) and RNF212 (H) is diminshed in *Rnf212b*$^{RING/RING}$ mutant meiocytes. Early pachytene spermatocyte nuclei from wild-type and *Rnf212b*$^{RING/RING}$ testes (left); and pachytene-stage nuclei from wild-type and *Rnf212b*$^{RING/RING}$

oocytes at E16.5 (right) were immunostained for SYCP3 and RNF212B (G) or RNF212 (H). Scale bars, 10 μm.

Figure 7. Summary of RNF212B, RNF212 and HEI10 functions in crossover regulation.

(A) Timing of the accumulation of RNF212B and RNF212, and appearance of HEI10 at prospective crossover sites relative to the substages of meiotic prophase-I. Accumulation of RNF212B is stronger and occurs earlier than its paralog RNF212 and is coincident with the appearance at HEI10.

(B) Schematic of RNF212B, RNF212, and HEI10 dynamics in the context of the SC highlighting dependencies defined here and previous studies [21-23,43,57,58]. RNF212 and RNF212B load in close association with the SC central region. Both DSBs and SC stabilize RNF212B. Repatterning of RNF212B and RNF212 requires HEI10 (this study), and possibly also cyclin-related CNTD1 and its partner PRR19, and cyclin-dependent kinase CDK2 [21-23,43,57,58]. The MutLγ complex, MLH1-MLH3, is important to confine HEI10 to differentiated crossover sites and for the full dissociation of RNF212, and to a lesser extent RNF212B, from noncrossover sites.

(C) Timing of the loss of RNF212B and RNF212 from noncrossover sites in spermatocytes. In

oocytes, numerous smaller foci of both proteins persist along SCs until they disassemble in diplotene.

(D) Models of crossover maturation and defects in *Rnf212b, Rnf212* and *Hei10* mutants. MutSγ complexes (grey rings) bind Holliday junctions and convert into sliding clamps that embrace the interacting duplexes [34]. At designated crossover sites, stabilization of MutSγ by RNF212, RNF212B, and HEI10 enables formation of double-Holliday junctions. An endonuclease-independent function of MutLγ is recently implicated in this step [63]. MutLγ-catalyzed incision and the Bloom complex (BLM-TOPIIIα-RMI1-RMI2; BTRR) then mediate crossover-specific resolution [15]. MutSγ is destabilized in *Rnf212b*$^{-/-}$, *Rnf212b*$^{RING/RING}$ and *Rnf212*$^{-/-}$ mutants exposing nascent intermediates to unwinding by the Bloom complex resulting in noncrossovers. In the *Hei10*$^{mei4/mei4}$ mutant, RNF212, RNF212B, and MutSγ persist at all sites throughout pachytene, and crossover sites fail to differentiate. DSBs are repaired as noncrossovers only as homologs desynapse and RNF212 and RNF212B dissociate.

SUPPLEMENTAL FIGURE LEGENDS

Figure S1. 5' UTR variants and isoforms of mouse *Rnf212b*, related to Figure 1.

(A) Protein sequence alignments of mouse and human RNF212B and RNF212 full-length isoforms. Zinc-coordinating cysteine and histidine (pink) residues of RING finger domain and other identical residues (blue) are highlighted.

(B) Schematic of 5' UTR variants and isoforms of mouse *Rnf212b*. Top, red and black bars represent 5' untranslated exons (5' UTRs) and coding exons, respectively. Bottom, yellow and blue boxes represent 5' UTRs and coding exons, respectively. For simplicity, 5' UTRs of isoforms a-c are not shown. Asterisks indicate positions of stop codons. Horizontal bars represent positions of primers used to detect each isoform by RT-PCR in (C). Annotated or related variants and isoforms in the NCBI database are also shown.

(C) Expression of mouse *Rnf212b* 5' UTR variants and isoforms analyzed by RT-PCR. Total RNA was extracted from indicated tissues of mature male mice and subjected to RT-PCR. *Gapdh* is a loading control.

Figure S2. Absence of crossover markers in *Rnf212b*$^{-/-}$ mutant mice, related to Figure 1.

Crossover-specific immunostaining foci of HEI10 (left), PRR19 (middle) and CDK2 (right) foci were absent from chromosome spreads of *Rnf212b*$^{-/-}$ spermatocytes. Mid/late pachytene nuclei

from wild-type and *Rnf212b*$^{-/-}$ spermatocytes were immunostained for SYCP3 plus HEI10 (left), PRR19 (middle), or CDK2 (right). The magnified images show representative chromosomes from the CDK2 staining. Note that CDK2 also localizes to telomeres, which is not affected by *Rnf212b* mutation. A white arrowhead indicates an interstitial CDK2 focus marking a prospective crossover site. Scale bars, 10 μm for images of full nuclei and 2 μm for magnified panels.

Figure S3. Normal synapsis except for the X-Y chromosomes in *Rnf212b*$^{-/-}$ mutant mice, related to Figure 1.

(A) Representative images of successive prophase-I stages in chromosome spreads of wild-type and *Rnf212b*$^{-/-}$ spermatocytes immunostained for SYCP3.

(B) Distributions of spermatocytes in successive prophase-I stages based on SYCP3 staining. >250 unselected SYCP3-positive cells were analyzed per mouse. Bar graphs indicate means of two mice with plots for each mouse. p = 0.001 for G test (total cells analyzed: 578 *Rnf212b*$^{+/+}$ cells and 549 *Rnf212b*$^{-/-}$ cells).

(C) Autosomal and X-Y synapsis in wild-type and *Rnf212b*$^{-/-}$ spermatocytes. Pachytene-stage spermatocyte nuclei immunostained for SYCP3 and H1t are shown. The magnified images show

X-Y chromosomes.

(D) Premature desynapsis of X-Y chromosomes in *Rnf212b*$^{-/-}$ and *Rnf212*$^{-/-}$ spermatocytes. ns, not significant ($p > 0.05$); ****$p \leq 0.0001$ for Fisher's exact tests. Total numbers of cells analyzed from 3 mice of each genotype are indicated below the X axis.

Scale bars, 10 μm for images of full nuclei and 2 μm for magnified panels.

Figure S4. Dynamics of RAD51 and DMC1 throughout zygonema and pachynema, related to Figure 2.

(A and B) Representative images of RAD51 (A) and DMC1 (B) immunostainings in wild-type and *Rnf212b*$^{-/-}$ spermatocytes nuclei immunostained for SYCP3 plus RAD51 (A) or DMC1 (B) at the indicated stages. White arrows indicate the X-Y chromosomes. Scale bars, 10 μm.

(C and D) Focus counts of RAD51 (C) and DMC1 (D). Red bars indicate means ± SDs. ns, not significant ($p > 0.05$); *$p \leq 0.05$; ***$p \leq 0.001$ for two-tailed Mann-Whitney tests. Total numbers of nuclei analyzed are indicated below the X axes.

Figure S5. Reduced numbers of TEX11 and MER3 foci in *Rnf212b*$^{-/-}$ mutant mice, related to

Figure 2.

(A and C) Images of wild-type and *Rnf212b*$^{-/-}$ spermatocyte nuclei immunostained for SYCP3 plus TEX11 (A) or MER3 (C) at the indicated stages. Scale bars, 10 μm.

(B and D) Counts of TEX11 (B) and MER3 (D) immunostaining foci. Red bars indicate means ± SDs. ****$p \leq 0.0001$ for two-tailed Mann-Whitney tests. Total numbers of nuclei analyzed are indicated below the X axes.

Figure S6. Specificity of anti-RNF212B antibody, related to Figure 3.

Wild-type and *Rnf212b*$^{-/-}$ spermatocyte nuclei at indicated stages were immunostained for SYCP3 and RNF212B. Scale bars, 10 μm.

Figure S7. RNF212B localization in prophase-I oocytes, related to Figure 3.

RNF212B localization at successive prophase-I stages of fetal oocyte nuclei from embryonic days 15.5 (E15.5) and 17.5 (E17.5), and 0.5 day postpartum (0.5 dpp). Surface-spread prophase-I oocyte nuclei were immunostained for SYCP3 and RNF212B. Orange arrowheads indicate large, differentiated RNF212B foci. The magnified images show representative

chromosomal regions. Scale bars, 10 μm for images of full nuclei and 2 μm for magnified panels.

Figure S8. Distinct localization patterns of differentiating RNF212B and RNF212 crossover foci, related to Figure 4.

(A) HEI10 forms crossover foci earlier than MLH1. Pachytene spermatocytes nuclei immunostained for SYCP3, HEI10, MLH1 and H1t. Top images show a representative H1t-negative, mid-pachytene nucleus in which small MLH1 foci are present on a minority chromosome (indicated by arrows) whereas bright HEI10 foci are present on all chromosomes. Bottom images show a representative H1t-psoitive late -pachytene nucleus in which both MLH1 and HEI10 form clear, overlapping crossover-specific foci on all chromosomes.

(B) Quantification of HEI10 and MLH1 foci in pachytene spermatocytes confirms that MLH1 foci develop only in nuclei with a full complement of HEI10 foci. 25 pachytene nuclei were randomly selected and analyzed.

(C) Quantification of focus intensities for RNF212B and RNF212. Each dot represents each focus of RNF212B and RNF212 from the early, mid and late pachytene nuclei analyzed in **Figure 4B**. Bars indicate means ± SDs. All, all foci; COs, crossover-specific foci that colocalize

with HEI10 foci; Others, foci that don't colocalize with HEI10 foci (noncrossover foci). ND, not detected. *$p \leq 0.05$; **$p \leq 0.01$; ****$p \leq 0.0001$ for two-tailed Mann-Whitney tests.

(D) Representation of per chromosome analysis of RNF212B and RNF212 foci for a mid-pachytene chromosome (shown in the images in the right-hand panels). Each focus of RNF212B or RNF212 is represented by a dot. The dashed line indicates the signal intensity of the brightest other focus (noncrossover focus) along the same chromosome. Orange vertical lines indicate the positions of HEI10-positive crossover sites (a) and (b). Intensities of foci at these sites relative to that of the brightest other (noncrossover) focus are: (a) 3.5 and (b) 2.3 for RNF212B; (a) 0.8 and (b) 1.1 for RNF212.

(E) Stronger differentiation of RNF212B than RNF212 at crossover sites in oocytes. Pachytene nuclei at embryonic day 18.5 (E18.5) immunostained for SYCP3, RNF212B, RNF212, and MLH1. The magnified images show representative chromosomes. Orange arrowheads indicate crossover sites.

Scale bars, 10 μm in images of full nuclei (A and E) and 2 μm in the magnified panels (D and E).

Figure S9. Timing of RNF212B focus differentiation and appearance of HEI10 foci, related

to Figure 4.

(A) Differentiation of RNF212B foci relative to the emergence of HEI10 foci. Airyscan images of an early-to-mid pachytene spermatocyte nucleus immunostained for SYCP3, RNF212B, RNF212 and HEI10. This nucleus contains 14 HEI10 foci indicating that it is in transition to full differentiation of crossovers sites (≥20 HEI10 foci). The white arrowhead indicates a differentiated RNF212B focus without an associated HEI10 focus; and the orange arrowhead indicates a differentiated RNF212B focus associated without a small, emerging HEI10 focus. These configurations indicate that growth of RNF212B foci can precede the emergence of HEI10 foci.

(B) Differentiation of RNF212B at crossover sites. Crossover-specific foci of RNF212B (i.e. RNF212B foci that colocalized with HEI10 foci) in early-to-mid pachytene nuclei (containing 5-18 HEI10 foci), and mid-pachytene nuclei (≥19 HEI10 foci) were classified based on their degree of differentiation by measuring their intensity relative to the brightest other (noncrossover) RNF212B focus along the same chromosome (complete differentiation, no other foci detected along the SC; strong differentiation, ≥2-fold brighter; weak differentiation, 1.5-2-fold brighter; or no differentiation, <1.5-fold brighter). 81 crossover-specific RNF212B foci from 7 early-to-mid

pachytene and 186 crossover-specific RNF212B foci from 8 mid-pachytene nuclei were analyzed by Airyscan imaging. In early-mid pachytene nuclei, the majority of HEI10 foci are associated with detectable differentiation of RNF212B, but 28% are not.

(C) Differentiation of RNF212B and emergence of HEI10 foci in early-to-mid pachynema. Numbers of HEI10 foci (sky blue), RNF212B foci with weak differentiation (yellow) and RNF212B foci with strong differentiation (orange) are shown. Criteria for RNF212B focus differentiation are as in (B). 71.6% (58/81 foci) of sites marked by HEI10 were coincident with weak or strong differentiation of RNF212B, while 78.4% (40/51 foci) of strongly differentiated RNF212B foci colocalized with a HEI10 focus. Thus, with respect to the differentiation of RNF212B and the emergence of HEI10 at prospective crossover sites, a sequential order of events is hard to discern and these events may be coincident, consistent with the dependence of RNF212B focus differentiation on HEI10. 7 early-to-mid pachytene nuclei with 5-18 HEI10 foci per nucleus were analyzed by Airyscan imaging.

Figure S10. Chromosomal localization of RNF212B and RNF212 in mutants defective for synapsis and crossing over, related to Figure 5.

(A) A mid zygotene-like *Sycp1*$^{-/-}$ spermatocyte nucleus immunostained for SYCP3, RNF212B, RNF212, and RPA2. General staining of RNF212B and RNF212 is absent but limited localization to small regions where homologous axes are closely aligned can be detected (magnified in the panels on the right).

(B and C) Quantification of RPA2 foci colocalizing with RNF212B and RNF212. (B) Degree of RNF212B and RNF212 colocalization with RPA2. (C) Quantification of total and colocalizing RPA2 foci. Black bars indicate means. 7 early-pachytene *Sycp1*$^{+/+}$ nuclei and 8 late-zygotene/early-pachytene-like *Sycp1*$^{-/-}$ nuclei were analyzed.

(D) Quantification of RNF212B-RNF212 colocalization. Black bars indicate means. 7 early pachytene *Sycp1*$^{+/+}$ nuclei and 8 late zygotene/early pachytene-like *Sycp1*$^{-/-}$ nuclei were analyzed.

(E) Normal chromosomal localization of RNF212B and RNF212 in early pachytene *Mlh3*$^{-/-}$ mutant spermatocyte nuclei. An early pachytene nucleus immunostained for SYCP3, RNF212B and RNF212 is shown.

(F) Numbers of RNF212B and RNF212 foci in wild-type and *Mlh3*$^{-/-}$ late-pachytene spermatocyte nuclei. Left, numbers of large and small RNF212B foci. Right, numbers of RNF212 foci

associated with crossover sites (colocalizing with large RNF212B foci) and other sites. Black bars indicate means. 20 *Mlh3*$^{+/+}$ and 18 *Mlh3*$^{-/-}$ nuclei were analyzed.

ns, not significant ($p > 0.05$); **$p \leq 0.01$; ***$p \leq 0.001$; ****$p \leq 0.0001$ for two-tailed Mann-Whitney tests. Scale bars, 10 µm in images of full nuclei (A and E) and 2 µm in the magnified panels (A).

Figure S11. Chromosomal localization of RNF212B and RNF212 in *Hei10* mutant spermatocytes, related to Figure 5.

(A) Persistent RNF212B staining in *Hei10*$^{mei4/mei4}$ spermatocytes. Images of a late-pachytene nucleus immunostained for SYCP3, RNF212B, RNF212 and H1t. The magnified panels show representative chromosomes with: (i) no apparent differentiation of RNF212B; or some differentiation, indicated by orange arrowheads. Scale bars, 10 µm in images of full nuclei and 2 µm in the magnified panels.

(B) Focus counts of RNF212B. Red bars indicate means. Total numbers of nuclei analyzed are indicated below the X-axis. For late stages, only late pachytene nuclei were analyzed for *Hei10*$^{+/+}$ whereas both late pachytene and early diplotene nuclei were analyzed for *Hei10*$^{mei4/mei4}$ because of the early desynapsis of *Hei10*$^{mei4/mei4}$ cells (Qiao et al., 2014). ns, not significant ($p > 0.05$);

****$p \leq 0.0001$ for two-tailed Mann-Whitney tests. Total numbers of nuclei analyzed are indicated below the X axis.

(C) Differentiation of RNF212B foci. Autosomes in late-pachytene *Hei10*$^{+/+}$ and *Hei10*$^{mei4/mei4}$ spermatocyte nuclei were categorized into four classes based on the degree of RNF212B differentiation. Strong, weak or no differentiation represents autosomes where the brightest RNF212B foci were ≥2-fold, 1.5-2-fold, or <1.5-fold brighter relative to the third brightest focus along the same synaptonemal complex, respectively. Complete differentiation is autosomes that have only one or two bright RNF212B foci. 8 late-pachytene *Hei10*$^{+/+}$ and 9 late-pachytene *Hei10*$^{mei4/mei4}$ nuclei were analyzed by Airyscan imaging. $p < 0.0001$ for a *G* test.

(D) Intensity of RNF212B foci at crossover sites relative to the brightest other focus along the same chromosome in late pachytene *Hei10*$^{mei4/mei4}$ and mid pachytene *Hei10*$^{+/+}$ spermatocyte nuclei. Red bars indicate means. Nuclei analyzed were the same as in (C) and **Figure 4E**, respectively. Total numbers of foci analyzed are indicated below the X-axis. ****$p \leq 0.0001$ for two-tailed Mann-Whitney test.

Figure S12. The RING finger domain is required for RNF212B function *in vivo*, related to

Figure 6.

(A) Scheme of the *Rnf212b* RING mutation. A three-nucleotides deletion in addition to a single-nucleotide substitution (shown in red) induced loss of the 9th cysteine residue with no change in other protein-coding amino acids. White and black boxes indicate 5' UTR and coding exons, respectively. The guide RNA (gRNA) sequence is highlighted in blue. Cysteine and histidine residues of RING finger domain are highlighted in pink.

(B) Reduced testis size in *Rnf212b*$^{RING/RING}$ mutants. Red bars indicate means. ns, not significant ($p > 0.05$); ****$p \leq 0.0001$ for two-tailed *t* tests. Numbers of mice analyzed are indicated below the X axis.

(C) Diminished chiasma numbers in *Rnf212b*$^{RING/RING}$ meiocytes. Left, wild-type and *Rnf212b*$^{RING/RING}$ spermatocytes in diakinesis/metaphase-I stages stained with DAPI. Right, metaphase-I oocytes from ≥2 months old wild-type and *Rnf212b*$^{RING/RING}$ females were stained with DAPI and immunostained for centromeres. Scale bars, 10 μm.

(D) Chiasma counts in *Rnf212b*$^{-/-}$ and *Rnf212b*$^{RING/RING}$ meiocytes. Red bars indicate means. ns, not significant ($p > 0.05$) for two-tailed Mann-Whitney tests. Total numbers of nuclei analyzed are indicated below the X axis.

(E) Absence of MLH1 foci in *Rnf212b*$^{RING/RING}$ spermatocytes. Mid-late pachytene nuclei from wild-type and *Rnf212b*$^{RING/RING}$ spermatocytes immunostained for SYCP3 and MLH1. Scale bars, 10 μm.

(F) High frequency of unpaired X-Y chromosomes in H1t-positive pachytene *Rnf212b*$^{RING/RING}$ cells. ns, not significant ($p > 0.05$); ****$p \leq 0.0001$ for fisher's exact tests. Total numbers of cells analyzed from 3 mice of each genotype are indicated below the X axis.

(G-J) Focus counts of RPA2 (G), MSH4 (H), TEX11 (I) and MER3 (J) in wild-type, *Rnf212b*$^{-/-}$, and *Rnf212b*$^{RING/RING}$ spermatocytes. Red bars indicate means ± SDs. ns, not significant ($p > 0.05$); *$p \leq 0.05$; **$p \leq 0.01$; ***$p \leq 0.001$; ****$p \leq 0.0001$ for two-tailed Mann-Whitney tests. Total numbers of nuclei analyzed are indicated below the X axes.

MATERIALS AND METHODS

Mice

Mice were maintained and euthanized according to the guidelines of the Institutional Animal Care and Use Committees of the University of California Davis. All mice were congenic with the C57BL/6J background except for *Sycp1*$^{-/-}$ mutant mice. The *Rnf212*$^{-/-}$, *Hei10*$^{mei4/mei4}$, *Spo11*$^{-/-}$,

Sycp1$^{-/-}$ and *Mlh3*$^{-/-}$ mutant lines were previously described [21,31,46,48,49]. Mature adult mice (2-6 months old) were used for experiments unless otherwise noted.

Rnf212b mutant alleles were generated by The Cornell Stem Cell and Transgenic Core Facility. 124 bp of DNA template for sgRNA, comprising the T7 polymerase binding site and sgRNA target sequence (5'-CCCCATCTTTTCGGAAACAC-3') followed by the remaining sgRNA sequence, were amplified by PCR as previously described [64] and purified using a GeneJET PCR Purification Kit (Thermo Scientific, K0702). 600 ng of purified DNA template was *in vitro* transcribed for 4 h at 37^{o}C using MEGAshortscript T7 Transcription Kit (Invitrogen, AM1354). sgRNA was purified using MEGAclear Transcription Clean-Up Kit (Invitrogen, AM1908), diluted to 1.6 µg/µl and stored at -80^{o}C prior to embryo injection. 12.5 ng/µl of purified sgRNA and either 12.5 or 25 ng/µl of Cas9 mRNA were microinjected into pronuclei of 2-cell stage of C57BL/6J homozygous embryos. Embryos were transferred to pseudo-pregnant female recipients 2 days after pronuclear injection at the 4-cell stage. Genomic DNA of founder mice was isolated from toe clips, PCR-amplified, cloned into the pCR4Blunt-TOPO vector (Invitrogen, 450031), and Sanger-sequenced to identify mutations. Founder mice were backcrossed to C57BL/6J mice for

≥4 generations and heterozygous mice were bred to homozygosity. Genotyping was performed by PCR on genomic DNA isolated from mouse tails. Primers used for cloning and genotyping are listed in **Table S2**.

Total RNA extraction, RT-PCR, and 5' RACE

Tissues were dissected from adult male mice, washed in phosphate-buffered saline (PBS), frozen in liquid nitrogen and stored at -80^{o}C prior to RNA extraction. Total RNA was extracted using TRIzol according to manufacturer's instructions (Invitrogen). 1 µg of total RNA was reverse-transcribed using the SuperScript IV First-Strand Synthesis System (Invitrogen, 18091050) and synthesized cDNA was PCR-amplified. For 5' RACE, 4 µg of total RNA from testes was reverse-transcribed using 5' RACE System for Rapid Amplification of cDNA Ends (Invitrogen, 18374058) and synthesized cDNA was PCR-amplified, cloned into the pCR4-TOPO TA vector (Invitrogen, K457501) and Sanger-sequenced to identify translation initiation site. Primers used are listed in **Table S2**.

Yeast two-hybrid assays

Full-length mouse *Rnf212b* and *Rnf212* cDNAs were amplified by PCR from mouse testis cDNA prepared as above and cloned into pGADT7 and pGBKT7 vectors (Clontech) using the Gibson Assembly Cloning Kit (NEB, E2611S). pGADT7-*Rnf212b*^{C9A}, pGADT7-*Rnf212*^{C10A}, and pGBKT7-*Rnf212b*^{C9A} vectors were generated using QuickChange Lightning Multi Site-Directed Mutagenesis Kit (Agilent Technologies, 210513). Y187 and Y2HGold yeast two-hybrid strains were transformed with vectors containing genes of interest or alone (empty vectors), mated on SD-Trp-Leu plates, and selection was performed on SD-Trp-Leu plates containing 200 ng/ml of Aureobasidin A (Clontech, 630466) according to the manufacturer's instructions (Clontech). Primers used for cloning and point mutagenesis are listed in **Table S2**.

Antibody production

Polyclonal antibodies against mouse RNF212B were raised in Guinea pigs. Codon-optimized of full-length mouse RNF212B was cloned into pET-28b (+) (Addgene) with a C-terminal 6xHis tag. *E. coli* Arctic Express (DE3) cells (Agilent Technologies Inc.) transformed with the mouse RNF212B-6xHis expression vector were grown in 2L of LB at 30^{o}C to an OD_{600} of 0.8, and protein expression was induced with 0.5 mM IPTG followed by incubation at 11^{o}C in media

supplemented with 0.1 mM $ZnCl_2$. ~5 g of cells were pelleted by centrifugation, suspended in 60 ml of denaturing lysis buffer A (6M Guanidine, 25 mM sodium-phosphate pH 7.4, 500 mM NaCl, 0.1 mM $ZnCl_2$, 1 mM β-mercaptoethanol, 20 mM imidazole, 10% glycerol) and sonicated. Samples were centrifuged at 35,000 rpm in a Ti-45 rotor (Beckman) for 45 min and soluble extract was applied to a 5 ml HisTrap FF column (GE healthcare Inc.) using a GE AKTA Avant 25 FPLC system. After equilibrating with 5 column volumes (CV) of lysis buffer A, followed by washes with 10 CV of wash buffer B (6M urea, 25 mM sodium-phosphate pH 7.4, 500 mM NaCl, 1 mM β-mercaptoethanol, 10% glycerol) supplemented with 60 mM imidazole, bound proteins were eluted with a linear gradient of imidazole (60-600 mM) in buffer B. Peak fractions were pooled and dialyzed extensively in decreasing urea concentrations (6M to 1M urea in 25 mM sodium-phosphate pH 7.4, 500 mM NaCl, 1 mM β-mercaptoethanol, 10% glycerol). Protein concentrations were determined by Bradford and spectrophotometric (A_{280}) methods. Two Guinea pigs were immunized with purified RNF212B protein by Antibodies Incorporated (Davis, CA). The IgG fraction was purified from the resultant sera, using the Montage antibody purification kit according to manufacturer's instructions (Millipore Sigma), and dialyzed against PBS containing 10% glycerol and aliquots stored at -80^{o}C.

Histology

Testes from adult male mice were dissected, punctured with a 27-guage needle, and fixed in 10% buffered formalin overnight at room temperature. Ovaries from 18 days postpartum (18 dpp) female mice were dissected and fixed in 10% buffered formalin overnight at room temperature. Fixed testes and ovaries were washed in PBS twice and stored in 70% ethanol at 4^{o}C prior to embedding. Tissues embedded in paraffin were sectioned (5 µm) onto glass slides (Fisher Scientific, 12-550-15), deparaffinized, rehydrated, and incubated with antigen retrieval buffer (10 mM Sodium Citrate, 0.05% Tween-20) for 50 min at 100^{o}C. Slides were then stained with hematoxylin and eosin (testes), or immunostained with anti-p63 antibody, as described below, and counterstained with hematoxylin (ovaries), and mounted with Permount (Fisher Scientific, SP15-100).

Surface spreads of spermatocyte chromosomes

Surface-spread chromosomes of spermatocytes were prepared as described previously [65]with slight modification. Testes were dissected, the tunica albuginea removed, and adherent

extratubular tissues removed by rinsing and dissociating seminiferous tubules in PBS using a pair of 25-gauge (adult) or 27-guage (juvenile) needles in a 35 mm petri dish (Corning, 430165). Dissociated seminiferous tubules were incubated in hypotonic extraction buffer (30 mM Tris-HCl pH 8.0, 50 mM sucrose, 17 mM trisodium citrate dihydrate, 5 mM EDTA, 0.5 mM dithiothreitol (DTT) and 0.5 mM phenylmethylsulphonyl fluoride (PMSF), pH 8.2-8.3) for 15-45 min at room temperature. After quickly rinsing seminiferous tubules in 100 mM sucrose, a small amount of tubules were placed in 40 µl of 100 mM sucrose on a glass depression slide. Tubules were torn to pieces using two fine forceps, and large pieces of tubular remnant were removed. The volume was increased to 40-60 µl by adding 100 mM sucrose and a cell suspension was made by pipetting. A clean glass slide (Fisher Scientific, 12-544-7) was dipped into freshly made PFA solution (1% paraformaldehyde adjusted to pH 9.2 using 1.25 M sodium borate, 0.15% Triton X-100) in a 50 ml Falcon tube, and excess solution was drained onto a paper towel. 20 µl of cell suspension was placed at the upper right corner of the slide and slowly dispersed in horizontal and vertical directions to homogeneously cover the slide. Hot tap water was added to a humid chamber and slides were slowly dried in the closed chamber overnight at room temperature. Slides were further dried for 3 hr with lid ajar, and then for 1-2 hr with the lid removed. Slides

were washed once for 5 min in deionized water and twice for 5 min in 0.4% Photo-Flo 200 solution (Kodak, 1464510) in a coplin jar before air-drying at room temperature. Slides were either directly processed for immunostaining, as described below, or stored wrapped in aluminum foil at -80^{o}C prior to immunostaining. For SIM imaging, 15 µl of cell suspension was placed at the upper right corner of a coverslip (Fisher Scientific, 12-544-E) coated with 90 µl of 1% PFA, 0.15% Triton X-100 solution and slowly dispersed as above.

Surface spreads of oocyte chromosomes

Surface-spread oocyte chromosomes were prepared as described for spermatocytes with modifications. Ovaries from fetal females were dissected into PBS and kept on ice prior to incubation in hypotonic extraction buffer. A pair of ovaries were incubated in hypotonic extraction buffer for 10 min at room temperature, quickly rinsed in 100 mM sucrose, and placed in 50 µl of 100 mM sucrose on a glass depression slide. Ovaries were torn to pieces using a pair of 25-guage needles, and large pieces of ovarian remnant were removed. The volume was increased to 40 µl by adding 100 mM sucrose and a cell suspension was made by pipetting. One half of a clean glass slide was coated with 50 µl of freshly made 1% PFA 0.15% Triton X-100, and

10 µl of cells suspension was placed at the upper right corner of the slide slowly dispersed in horizontal and vertical directions to homogeneously cover the half slide. Slides were then dried, washed, and stored as described for spermatocyte chromosomes spreads.

Chromosome spreads of diakinesis/metaphase-I spermatocytes

Testes from adult male mice were dissected, tunica albuginea removed, and seminiferous tubules placed in 2 ml of hypotonic solution (1% trisodium citrate) in a 35 mm petri dish. Seminiferous tubules were torn to pieces using two fine forceps and, after adding 1 ml of hypotonic solution, 3 ml of tubule suspension was transferred to a 15 ml Falcon tube using a plastic transfer pipette (Phenix, PP-137030). Tubule fragments were allowed to settle out for 3 min and the supernatant containing suspended cells was transferred to another 15 ml Falcon tube. Remnant tubule fragments in the petri dish were suspended in 2 ml of hypotonic solution and transferred to the first 15 ml Falcon tube containing tubule fragments. The mixture of tubule fragments was resuspended using a transfer pipette, tubule fragments were settled out, and the supernatant was transferred to the 15 ml Falcon tube containing the first supernatant. The mixture of supernatants was filtered through 70 µm and 40 µm Cell Strainers (Corning 352350;

Celltreat, 229481) and suspended cells were pelleted by centrifugation at 900 rpm for 10 min at room temperature. Cells were fixed by adding 3 ml of freshly made fixative solution 1 (75% methanol, 25% acetic acid with 0.375% chloroform) drop-by-drop while gentle vortexing. Cells pelleted by centrifugation at 900 rpm for 10 min at room temperature, resuspended in 3 ml of freshly made fixative solution 2 (75% methanol, 25% acetic acid, chilled to -20^{o}C), pelleted again, and resuspended in 0.5 ml of fixative solution 2. Fixed cell suspension was dropped onto a clean glass slide (Fisher Scientific, 12-544-7) from a height of 2-3 feet height using a glass Pasteur pipette in a room with >40% humidity. Slides were air-dried for 10 min at room temperature and either stained immediately with ProLong Gold or Diamond Antifade Mountant (Thermo Fisher Scientific, P36930 or P36970) containing 1 µg/ml DAPI, or stored at 4^{o}C prior to staining.

Chromosome spreads of metaphase-I oocytes

Ovaries from adult female mice without prior hormonal stimulation were dissected, follicles were punctured in pre-warmed (37^{o}C) M2 media (Sigma-Aldrich, M7167) using a 25-gauge needle, and germinal-vesicle stage oocytes with integral cumulus cell layers were collected. Surrounding cumulus cells were mechanically removed by pipetting and oocytes were cultured in M2 media

for 7 hr at 37^{o}C. Metaphase-I oocytes were transferred into Tyrode's acidic solution (Sigma-Aldrich, T1788) to remove the zona pellucida (ZP), and ZP-free oocytes were transferred and maintained in M2 media prior to spreading. 5-10 µl of 1% PFA solution pH 9.2 containing 0.15% Triton X-100 and 3 mM DTT was placed in each well of a 12-well glass slide (Electron Microscopy Sciences, 63425-05) and one ZP-free oocyte was transferred to each well. Slides were air-dried overnight at room temperature, and either directly processed for immunostaining or stored at 4^{o}C for up to several days prior to immunostaining.

Immunostaining

Slides were rehydrated with Tris-buffered saline (TBS) pH 8.0 containing 0.05% of Triton X-100 (TBST) for 3 min, blocked twice with blocking buffer (1% normal goat or donkey serum, 3% bovine serum albumin (BSA), 1x TBS pH 8.0, 0.05% Triton X-100, 0.05% sodium azide) for 15 min at room temperature and incubated with primary antibodies in antibody dilution buffer (10% normal goat or donkey serum, 3% BSA, 1x TBS pH 8.0, 0.05% Triton X-100, 0.05% sodium azide) in a humid chamber overnight at room temperature. Slides were briefly rinsed with TBST, washed twice with TBST for 5 min, blocked twice with blocking buffer for 15 min at room

temperature and then incubated with secondary antibodies in antibody dilution buffer in a humid chamber for 1 hr at 37^{o}C. Slides were rinsed with TBST, washed three times with TBST for 5 min, washed once with Milli-Q water for 2 min, and air-dried prior to mounting with ProLong Gold or Diamond Antifade Mountant. For SIM imaging, cover slips were blocked three times for 15 min prior to primary antibody incubation.

For metaphase-I oocytes, slides were briefly rehydrated with TBST, washed three times with TBST for 5 min, blocked twice with blocking buffer for 15 min at room temperature, and incubated with primary antibodies in antibody dilution buffer in a humid chamber overnight at room temperature. Slides were rinsed with TBST, briefly washed twice with TBST, blocked twice with blocking buffer for 15 min at room temperature, and incubated with secondary antibodies in antibody dilution buffer in a humid chamber for 1 hr at room temperature. Slides were rinsed with TBST, briefly washed with TBST, and then washed three times with TBST for 5 min. Slides were then incubated with TBST containing 5 µg/ml DAPI for 10 min at room temperature and mounted with 50% ProLong Gold or Diamond Antifade Mountant in TBST.

All primary and secondary antibodies used are listed in **Table S3**.

Protein blot analysis

Testes were dissected from 18 dpp juvenile male mice, frozen in liquid nitrogen, and stored at -80^{o}C prior to cell lysis. Five pairs of testes were homogenized in 1 mL RIPA buffer (50 mM Tris-HCl pH 7.5, 150 mM NaCl, 1 mM EDTA, 1% NP-40, 0.5% sodium deoxycholate, 0.1% sodium dodecyl sulfate, SDS) supplemented with protease and isopeptidase inhibitors (1x Complete protease inhibitor EDTA-free, Roche, 04693159001), 1 mM PMSF, 10 mM N-ethylmaleimide, NEM) on ice, incubated for 15 min on ice, sonicated with a setting of 20% duty cycle and output 2 on and off for 2.5 min, and then incubated for 15 min on ice. The samples were centrifuged at 14,000 rpm for 15 min at 4^{o}C and supernatants were collected as whole-testis extracts. Protein concentrations were measured by Bradford assay and normalized between samples by adding RIPA buffer supplemented with protease and isopeptidase inhibitors. Whole-testis extract was subjected to immunoprecipitation or mixed with 4x SDS-PAGE loading buffer (250 mM Tris-HCl pH 6.8, 8% SDS, 40% glycerol, 572 mM β-mercaptoethanol, 0.05% bromophenol blue), boiled for 5 min at 100^{o}C and subjected to electrophoresis and

immunoblotting. For immunoprecipitation, whole-testis extract containing 10-11 mg of total protein was incubated with 10 µl of anti-RNF212B antibody overnight at 4^{o}C with end-over-end rotation. Protein G Sepharose 4 Fast Flow (GE Healthcare, 17061801) was equilibrated with PBS containing 0.5% BSA, and 20 µl of 50% beads suspension was added to the samples. After incubation for 2 hr at 4^{o}C with end-over-end rotation, beads were washed three times with RIPA buffer, resuspended in 4x SDS-PAGE loading buffer and boiled for 5 min at 100^{o}C.

Protein samples were separated on 10% gels by SDS-PAGE and transferred to nitrocellulose membranes by wet transfer method in Towbin buffer (25 mM Tris, 192 mM glycine, 20% methanol) at 60 V for 150 min at 4^{o}C. Membranes were blocked with PBS containing 2.5 % non-fat milk for 1 h at room temperature and incubated with primary antibodies in 2.5 % non-fat milk in PBS overnight at 4^{o}C. Membranes were washed three times with PBS containing 0.05% Tween-20 (PBST) for 10 min and incubated with HRP-conjugated secondary antibodies in PBST for 1 hr at room temperature. Membranes were washed three times with PBST for 10 min and the signal was developed using the SuperSignal West Pico Chemiluminescent Substrate (Thermo Scientific, PI-34080) and detected using an Amersham Imager 600 (GE Healthcare).

All primary and HRP-conjugated secondary antibodies used are listed in **Table S3**.

Image acquisition

Images of surface-spread prophase chromosomes and metaphase-I chromosome spreads were acquired using a Zeiss AxioPlan II microscope with a 63 x Plan-Apochromat 1.4 NA objective and EXFO X-Cite metal halide light source, captured with a Hamamatsu ORCA-ER CCD camera and processed using Volocity (Perkin Elmer) and Photoshop (Adobe) software. SIM images were acquired using a Nikon N-SIM super-resolution microscope and processed using NIS-Elements 2 image processing software. Airyscan images were acquired using a Zeiss LSM800 with Airyscan microscope with a 60 x 1.4 NA objective and processed using ZEN imaging software (Carl Zeiss). Images of testis sections were acquired using a Zeiss Axio Imager M2 microscope with a 20 x Plan-Apochromat 0.8 NA objective, captured with a Hamamatsu ORCA-Flash 4.0 V3 sCMOS camera and processed using ZEN imaging software (Carl Zeiss). Images of ovary sections were acquired using a ScanScope digital scanner (Asperio) and processed using ImageScope software.

Image analysis

Comparisons were made between animals that were either littermates or matched by age. Numbers and colocalization of foci were determined manually. *Rnf212b*$^{-/-}$, *Rnf212*$^{-/-}$ and *Rnf212b*$^{RING/RING}$ mutant analysis was blinded with respect to the genotype of the animals. Results from more ≥2 independent experiments/animals were pooled for quantification of number of foci and chiasmata. *Spo11*$^{-/-}$, *Sycp1*$^{-/-}$, *Mlh3*$^{-/-}$ and *Hei10*$^{mei4/mei4}$ mutant analysis was not blinded to genotype because phenotypes are overt. For focus intensity analyses, RNF212B and RNF212 foci along homolog axes were automatically defined by thresholding intensity on SYCP3 staining and manually inspecting images to separate any adjacent focus pairs defined as one focus. For *Spo11*$^{-/-}$ mutant analysis, synapsed regions marked by SYCP1 were manually cropped and intensities of RNF212B and RNF212 were measured. Two regions of interest (ROI) were drawn inside nuclei but adjacent to homolog axes and their average intensity was subtracted as background for each nucleus. Results from one experiment/animal among ≥2 independent experiments/animals were shown for quantification of intensities.

Prophase-I stages were defined by SYCP3 staining (spermatocytes) and both SYCP3 staining and fetal age (oocytes) using standard criteria. Leptonema was defined by short SYCP3 stretches without evidence of synapsis determined by thickening of SYCP3 staining. Zygonema was defined by longer stretches of SYCP3 with various degree of synapsis: early, mid- and late-zygonema were defined by having <25%, 25-75% and >75% of synapsis, respectively. Pachynema was defined by full synapsis of all autosomes. For spermatocytes, early pachynema was defined by extensive synapsis between the X-Y chromosomes, mid pachynema was defined by limited/end-to-end X-Y synapsis, and late pachynema was defined by decondensed/elongated X-Y chromosomes with figure-of eight configuration and thickening of SYCP3 staining at telomeres of autosomes. Diplonema in spermatocytes was defined by internal desynapsis with various degrees of residual synapsis: early, mid and late diplonema were defined by having >75%, 75-25% and<25% of synapsis, respectively. For oocytes, nuclei with unsynapsed/desynapsed chromosomes at embryonic day 15.5 (E15.5) and at 0.5 day postpartum (0.5 dpp) were defined as zygonema and diplonema, respectively. Dictyate stage was defined by short, ragged SYCP3 stretches without evidence of synapsis at 0.5 dpp.

For ovary sections, numbers of oocytes were manually counted for every fifth section and counts were multiplied by five to calculate the total number of oocytes per pair of ovaries, as described previously [66].

Statistical analysis

Statistical analyses were performed using Graphpad Prism software v.8 and R version 3.5.2. Statistical parameters and tests, sample sizes, means, error bars, and standard deviations (SDs) are described in the figures and/or corresponding figure legends. Sample sizes were not predetermined using any statistical tests.

Acknowledgement

We thank M.A. Handel, P. Cohen, C. Höög, J. Ward, and R.J. Pezza for antibodies; the UC Davis MCB Light Microscopy Imaging Facility and M.R. Paddy for help with SIM imaging; the Cornel Stem Cell and Transgenic Core Facility, supported in part by Empire State Stem Cell Fund Contract Number C024174, J. Schimenti and R.J. Munroe for generating *Rnf212b* mutant mice; and members of the Hunter lab for helpful discussions. M.I. was supported by a Japan

Society for the Promotion of Science postdoctoral fellowship for research abroad. S.S. was supported by A.P. Giannini postdoctoral fellowship. B.N. was supported by the Howard Hughes Medical Institute EXROP program. N.H. is an Investigator with the Howard Hughes Medical Institute.

Author contributions

M.I. and N.H. conceived the study and designed the experiments. M.I., L.H., K.L., N.L., R.H., R.P., C.H., and I.H. performed the experiments and analyzed the data. Y.Y. performed oocyte culture experiments and analyzed the data. S.S. and B.N. performed histological experiments and analyzed the data. D.S.K. generated anti-RNF212B antibodies. M.I. and N.H. wrote the manuscripts with input from Y.Y., S.S., and D.S.K. All of authors edited the manuscript.

Competing financial interests

The authors declare no competing financial interests.

REFERENCES

1. Watanabe, Y. (2012). Geometry and force behind kinetochore orientation: lessons from meiosis. Nat Rev Mol Cell Biol *13*, 370-382. 10.1038/nrm3349.

2. Hunter, N. (2015). Meiotic Recombination: The Essence of Heredity. Cold Spring Harb Perspect Biol *7*. 10.1101/cshperspect.a016618.

3. Zickler, D., and Kleckner, N. (2023). Meiosis: Dances Between Homologs. Annu Rev Genet. 10.1146/annurev-genet-061323-044915.

4. Faisal, I., and Kauppi, L. (2017). Reduced MAD2 levels dampen the apoptotic response to non-exchange sex chromosomes and lead to sperm aneuploidy. Development *144*, 1988-1996. 10.1242/dev.149492.

5. Hassold, T., Hall, H., and Hunt, P. (2007). The origin of human aneuploidy: where we have been, where we are going. Human molecular genetics *16 Spec No. 2*, R203-208.

6. Hassold, T., and Hunt, P. (2001). To err (meiotically) is human: the genesis of human aneuploidy. Nat Rev Genet *2*, 280-291.

7. Faisal, I., and Kauppi, L. (2016). Sex chromosome recombination failure, apoptosis, and fertility in male mice. Chromosoma *125*, 227-235. 10.1007/s00412-015-0542-9.

8. Hassold, T., Maylor-Hagen, H., Wood, A., Gruhn, J., Hoffmann, E., Broman, K.W., and

Hunt, P. (2021). Failure to recombine is a common feature of human oogenesis. Am J Hum Genet *108*, 16-24. 10.1016/j.ajhg.2020.11.010.

9. Wang, S., Hassold, T., Hunt, P., White, M.A., Zickler, D., Kleckner, N., and Zhang, L. (2017). Inefficient Crossover Maturation Underlies Elevated Aneuploidy in Human Female Meiosis. Cell *168*, 977-989 e917. 10.1016/j.cell.2017.02.002.

10. Wartosch, L., Schindler, K., Schuh, M., Gruhn, J.R., Hoffmann, E.R., McCoy, R.C., and Xing, J. (2021). Origins and mechanisms leading to aneuploidy in human eggs. Prenat Diagn *41*, 620-630. 10.1002/pd.5927.

11. Lam, I., and Keeney, S. (2014). Mechanism and regulation of meiotic recombination initiation. Cold Spring Harb Perspect Biol *7*, a016634. 10.1101/cshperspect.a016634.

12. Brown, M.S., and Bishop, D.K. (2014). DNA strand exchange and RecA homologs in meiosis. Cold Spring Harb Perspect Biol *7*, a016659. 10.1101/cshperspect.a016659.

13. Cole, F., Kauppi, L., Lange, J., Roig, I., Wang, R., Keeney, S., and Jasin, M. (2012). Homeostatic control of recombination is implemented progressively in mouse meiosis. Nature cell biology *14*, 424-430. 10.1038/ncb2451.

14. Zakharyevich, K., Tang, S., Ma, Y., and Hunter, N. (2012). Delineation of joint molecule

resolution pathways in meiosis identifies a crossover-specific resolvase. Cell *149*, 334-347. 10.1016/j.cell.2012.03.023.

15. Kulkarni, D.S., Owens, S.N., Honda, M., Ito, M., Yang, Y., Corrigan, M.W., Chen, L., Quan, A.L., and Hunter, N. (2020). PCNA activates the MutLgamma endonuclease to promote meiotic crossing over. Nature. 10.1038/s41586-020-2645-6.

16. Cannavo, E., Sanchez, A., Anand, R., Ranjha, L., Hugener, J., Adam, C., Acharya, A., Weyland, N., Aran-Guiu, X., Charbonnier, J.B., et al. (2020). Regulation of the MLH1-MLH3 endonuclease in meiosis. Nature. 10.1038/s41586-020-2592-2.

17. Adams, I.R., and Davies, O.R. (2023). Meiotic Chromosome Structure, the Synaptonemal Complex, and Infertility. Annu Rev Genomics Hum Genet *24*, 35-61. 10.1146/annurev-genom-110122-090239.

18. Wang, S., Zickler, D., Kleckner, N., and Zhang, L. (2015). Meiotic crossover patterns: obligatory crossover, interference and homeostasis in a single process. Cell cycle *14*, 305-314. 10.4161/15384101.2014.991185.

19. Chelysheva, L., Vezon, D., Chambon, A., Gendrot, G., Pereira, L., Lemhemdi, A., Vrielynck, N., Le Guin, S., Novatchkova, M., and Grelon, M. (2012). The Arabidopsis

HEI10 is a new ZMM protein related to Zip3. PLoS genetics *8*, e1002799. 10.1371/journal.pgen.1002799.

20. Cheng, C.H., Lo, Y.H., Liang, S.S., Ti, S.C., Lin, F.M., Yeh, C.H., Huang, H.Y., and Wang, T.F. (2006). SUMO modifications control assembly of synaptonemal complex and polycomplex in meiosis of Saccharomyces cerevisiae. Genes & development *20*, 2067-2081. 10.1101/gad.1430406.

21. Reynolds, A., Qiao, H., Yang, Y., Chen, J.K., Jackson, N., Biswas, K., Holloway, J.K., Baudat, F., de Massy, B., Wang, J., et al. (2013). RNF212 is a dosage-sensitive regulator of crossing-over during mammalian meiosis. Nat Genet *45*, 269-278. 10.1038/ng.2541.

22. Qiao, H., Prasada Rao, H.B., Yang, Y., Fong, J.H., Cloutier, J.M., Deacon, D.C., Nagel, K.E., Swartz, R.K., Strong, E., Holloway, J.K., et al. (2014). Antagonistic roles of ubiquitin ligase HEI10 and SUMO ligase RNF212 regulate meiotic recombination. Nat Genet *46*, 194-199. 10.1038/ng.2858.

23. Rao, H.B., Qiao, H., Bhatt, S.K., Bailey, L.R., Tran, H.D., Bourne, S.L., Qiu, W., Deshpande, A., Sharma, A.N., Beebout, C.J., et al. (2017). A SUMO-ubiquitin relay recruits proteasomes to chromosome axes to regulate meiotic recombination. Science

355, 403-407. 10.1126/science.aaf6407.

24. De Muyt, A., Zhang, L., Piolot, T., Kleckner, N., Espagne, E., and Zickler, D. (2014). E3 ligase Hei10: a multifaceted structure-based signaling molecule with roles within and beyond meiosis. Genes & development *28*, 1111-1123. 10.1101/gad.240408.114.

25. Zhang, L., Kohler, S., Rillo-Bohn, R., and Dernburg, A.F. (2018). A compartmentalized signaling network mediates crossover control in meiosis. Elife *7*, e30789 doi: 30710.37554/eLife.30789. 10.7554/eLife.30789.

26. Nguyen, H., Labella, S., Silva, N., Jantsch, V., and Zetka, M. (2018). C. elegans ZHP-4 is required at multiple distinct steps in the formation of crossovers and their transition to segregation competent chiasmata. PLoS genetics *14*, e1007776. 10.1371/journal.pgen.1007776.

27. Lake, C.M., Nielsen, R.J., Bonner, A.M., Eche, S., White-Brown, S., McKim, K.S., and Hawley, R.S. (2019). Narya, a RING finger domain-containing protein, is required for meiotic DNA double-strand break formation and crossover maturation in Drosophila melanogaster. PLoS genetics *15*, e1007886. 10.1371/journal.pgen.1007886.

28. Wang, K., Wang, M., Tang, D., Shen, Y., Miao, C., Hu, Q., Lu, T., and Cheng, Z. (2012).

The role of rice HEI10 in the formation of meiotic crossovers. PLoS genetics *8*, e1002809. 10.1371/journal.pgen.1002809.

29. Lake, C.M., Nielsen, R.J., Guo, F., Unruh, J.R., Slaughter, B.D., and Hawley, R.S. (2015). Vilya, a component of the recombination nodule, is required for meiotic double-strand break formation in Drosophila. Elife *4*, e08287. 10.7554/eLife.08287.

30. Bhalla, N., Wynne, D.J., Jantsch, V., and Dernburg, A.F. (2008). ZHP-3 acts at crossovers to couple meiotic recombination with synaptonemal complex disassembly and bivalent formation in C. elegans. PLoS genetics *4*, e1000235. 10.1371/journal.pgen.1000235.

31. Ward, J.O., Reinholdt, L.G., Motley, W.W., Niswander, L.M., Deacon, D.C., Griffin, L.B., Langlais, K.K., Backus, V.L., Schimenti, K.J., O'Brien, M.J., et al. (2007). Mutation in mouse hei10, an e3 ubiquitin ligase, disrupts meiotic crossing over. PLoS genetics *3*, e139. 10.1371/journal.pgen.0030139.

32. Shinohara, M., Oh, S.D., Hunter, N., and Shinohara, A. (2008). Crossover assurance and crossover interference are distinctly regulated by the ZMM proteins during yeast meiosis. Nat Genet *40*, 299-309.

33. Pyatnitskaya, A., Borde, V., and De Muyt, A. (2019). Crossing and zipping: molecular

duties of the ZMM proteins in meiosis. Chromosoma *128*, 181-198. 10.1007/s00412-019-00714-8.

34. Snowden, T., Acharya, S., Butz, C., Berardini, M., and Fishel, R. (2004). hMSH4-hMSH5 recognizes Holliday Junctions and forms a meiosis-specific sliding clamp that embraces homologous chromosomes. Molecular cell *15*, 437-451.

35. Jessop, L., Rockmill, B., Roeder, G.S., and Lichten, M. (2006). Meiotic chromosome synapsis-promoting proteins antagonize the anti-crossover activity of Sgs1. PLoS genetics *2*, e155.

36. De Muyt, A., Jessop, L., Kolar, E., Sourirajan, A., Chen, J., Dayani, Y., and Lichten, M. (2012). BLM helicase ortholog Sgs1 is a central regulator of meiotic recombination intermediate metabolism. Molecular cell *46*, 43-53. 10.1016/j.molcel.2012.02.020.

37. Tang, S., Wu, M.K.Y., Zhang, R., and Hunter, N. (2015). Pervasive and essential roles of the Top3-Rmi1 decatenase orchestrate recombination and facilitate chromosome segregation in meiosis. Molecular cell *57*, 607-621. 10.1016/j.molcel.2015.01.021.

38. Johnston, S.E., Berenos, C., Slate, J., and Pemberton, J.M. (2016). Conserved Genetic Architecture Underlying Individual Recombination Rate Variation in a Wild Population of

Soay Sheep (Ovis aries). Genetics *203*, 583-598. 10.1534/genetics.115.185553.

39. Johnston, S.E., Huisman, J., and Pemberton, J.M. (2018). A Genomic Region Containing REC8 and RNF212B Is Associated with Individual Recombination Rate Variation in a Wild Population of Red Deer (Cervus elaphus). G3 (Bethesda) *8*, 2265-2276. 10.1534/g3.118.200063.

40. Kadri, N.K., Harland, C., Faux, P., Cambisano, N., Karim, L., Coppieters, W., Fritz, S., Mullaart, E., Baurain, D., Boichard, D., et al. (2016). Coding and noncoding variants in HFM1, MLH3, MSH4, MSH5, RNF212, and RNF212B affect recombination rate in cattle. Genome Res *26*, 1323-1332. 10.1101/gr.204214.116.

41. Johnston, S.E., Stoffel, M.A., and Pemberton, J.M. (2020). Variants at RNF212 and RNF212B are associated with recombination rate variation in Soay sheep (Ovis aries). bioRxiv, 2020.2007.2026.217802. 10.1101/2020.07.26.217802.

42. Gershoni, M., Braun, T., Hauser, R., Barda, S., Lehavi, O., Malcov, M., Frumkin, T., Kalma, Y., Pietrokovski, S., Arama, E., and Kleiman, S.E. (2023). A pathogenic variant in the uncharacterized RNF212B gene results in severe aneuploidy male infertility and repeated

IVF failure. HGG Adv *4*, 100189. 10.1016/j.xhgg.2023.100189.

43. Bondarieva, A., Raveendran, K., Telychko, V., Rao, H., Ravindranathan, R., Zorzompokou, C., Finsterbusch, F., Dereli, I., Papanikos, F., Trankner, D., et al. (2020). Proline-rich protein PRR19 functions with cyclin-like CNTD1 to promote meiotic crossing over in mouse. Nat Commun *11*, 3101. 10.1038/s41467-020-16885-3.

44. Ashley, T., Walpita, D., and de Rooij, D.G. (2001). Localization of two mammalian cyclin dependent kinases during mammalian meiosis. Journal of cell science *114*, 685-693.

45. Hinch, A.G., Becker, P.W., Li, T., Moralli, D., Zhang, G., Bycroft, C., Green, C., Keeney, S., Shi, Q., Davies, B., and Donnelly, P. (2020). The Configuration of RPA, RAD51, and DMC1 Binding in Meiosis Reveals the Nature of Critical Recombination Intermediates. Molecular cell *79*, 689-701 e610. 10.1016/j.molcel.2020.06.015.

46. Baudat, F., Manova, K., Yuen, J.P., Jasin, M., and Keeney, S. (2000). Chromosome synapsis defects and sexually dimorphic meiotic progression in mice lacking Spo11. Molecular cell *6*, 989-998.

47. Romanienko, P.J., and Camerini-Otero, R.D. (2000). The mouse Spo11 gene is required for meiotic chromosome synapsis. Molecular cell *6*, 975-987.

48. de Vries, F.A., de Boer, E., van den Bosch, M., Baarends, W.M., Ooms, M., Yuan, L., Liu, J.G., van Zeeland, A.A., Heyting, C., and Pastink, A. (2005). Mouse Sycp1 functions in synaptonemal complex assembly, meiotic recombination, and XY body formation. Genes & development *19*, 1376-1389.

49. Lipkin, S.M., Moens, P.B., Wang, V., Lenzi, M., Shanmugarajah, D., Gilgeous, A., Thomas, J., Cheng, J., Touchman, J.W., Green, E.D., et al. (2002). Meiotic arrest and aneuploidy in MLH3-deficient mice. Nat Genet *31*, 385-390.

50. Brzovic, P.S., Rajagopal, P., Hoyt, D.W., King, M.C., and Klevit, R.E. (2001). Structure of a BRCA1-BARD1 heterodimeric RING-RING complex. Nat Struct Biol *8*, 833-837. 10.1038/nsb1001-833.

51. Morgan, C., Fozard, J.A., Hartley, M., Henderson, I.R., Bomblies, K., and Howard, M. (2021). Diffusion-mediated HEI10 coarsening can explain meiotic crossover positioning in Arabidopsis. Nat Commun *12*, 4674. 10.1038/s41467-021-24827-w.

52. Fozard, J.A., Morgan, C., and Howard, M. (2023). Coarsening dynamics can explain meiotic crossover patterning in both the presence and absence of the synaptonemal complex. Elife *12*. 10.7554/eLife.79408.

53. Zhang, L., Stauffer, W., Zwicker, D., A.F., D., and (2021). Crossover patterning through kinase-regulated condensation and coarsening of recombination nodules. bioRxiv *2021.08.26.457865*. https://doi.org/10.1101/2021.08.26.457865

54. Kleckner, N., Zickler, D., Jones, G.H., Dekker, J., Padmore, R., Henle, J., and Hutchinson, J. (2004). A mechanical basis for chromosome function. Proc Natl Acad Sci U S A *101*, 12592-12597. 10.1073/pnas.0402724101.

55. Zhang, L., Liang, Z., Hutchinson, J., and Kleckner, N. (2014). Crossover patterning by the beam-film model: analysis and implications. PLoS genetics *10*, e1004042. 10.1371/journal.pgen.1004042.

56. McMahill, M.S., Sham, C.W., and Bishop, D.K. (2007). Synthesis-dependent strand annealing in meiosis. PLoS biology *5*, e299.

57. Palmer, N., Talib, S.Z.A., Singh, P., Goh, C.M.F., Liu, K., Schimenti, J.C., and Kaldis, P. (2020). A novel function for CDK2 activity at meiotic crossover sites. PLoS biology *18*, e3000903. 10.1371/journal.pbio.3000903.

58. Holloway, J.K., Sun, X., Yokoo, R., Villeneuve, A.M., and Cohen, P.E. (2014). Mammalian CNTD1 is critical for meiotic crossover maturation and deselection of excess

precrossover sites. J Cell Biol *205*, 633-641. 10.1083/jcb.201401122.

59. Qiao, H., Chen, J.K., Reynolds, A., Höög, C., Paddy, M., and Hunter, N. (2012). Interplay between synaptonemal complex, homologous recombination, and centromeres during mammalian meiosis. PLoS genetics *8*, e1002790. 10.1371/journal.pgen.1002790.

60. Serrentino, M.E., Chaplais, E., Sommermeyer, V., and Borde, V. (2013). Differential association of the conserved SUMO ligase Zip3 with meiotic double-strand break sites reveals regional variations in the outcome of meiotic recombination. PLoS genetics *9*, e1003416. 10.1371/journal.pgen.1003416.

61. van der Heijden, G.W., Derijck, A.A., Posfai, E., Giele, M., Pelczar, P., Ramos, L., Wansink, D.G., van der Vlag, J., Peters, A.H., and de Boer, P. (2007). Chromosome-wide nucleosome replacement and H3.3 incorporation during mammalian meiotic sex chromosome inactivation. Nat Genet *39*, 251-258. 10.1038/ng1949.

62. Ghafari, F., Gutierrez, C.G., and Hartshorne, G.M. (2007). Apoptosis in mouse fetal and neonatal oocytes during meiotic prophase one. BMC Dev Biol *7*, 87. 10.1186/1471-213X-7-87.

63. Premkumar, T., Paniker, L., Kang, R., Biot, M., Humphrey, E., Destain, H., Ferranti, I.,

Okulate, I., Nguyen, H., Kilaru, V., et al. (2023). Genetic dissection of crossover mutants defines discrete intermediates in mouse meiosis. Molecular cell *83*, 2941-2958 e2947. 10.1016/j.molcel.2023.07.022.

64. Bassett, A.R., Tibbit, C., Ponting, C.P., and Liu, J.L. (2013). Highly efficient targeted mutagenesis of Drosophila with the CRISPR/Cas9 system. Cell Rep *4*, 220-228. 10.1016/j.celrep.2013.06.020.

65. Peters, A.H., Plug, A.W., van Vugt, M.J., and de Boer, P. (1997). A drying-down technique for the spreading of mammalian meiocytes from the male and female germline. Chromosome Res *5*, 66-68.

66. Di Giacomo, M., Barchi, M., Baudat, F., Edelmann, W., Keeney, S., and Jasin, M. (2005). Distinct DNA-damage-dependent and -independent responses drive the loss of oocytes in recombination-defective mouse mutants. Proc Natl Acad Sci U S A *102*, 737-742. 10.1073/pnas.0406212102.

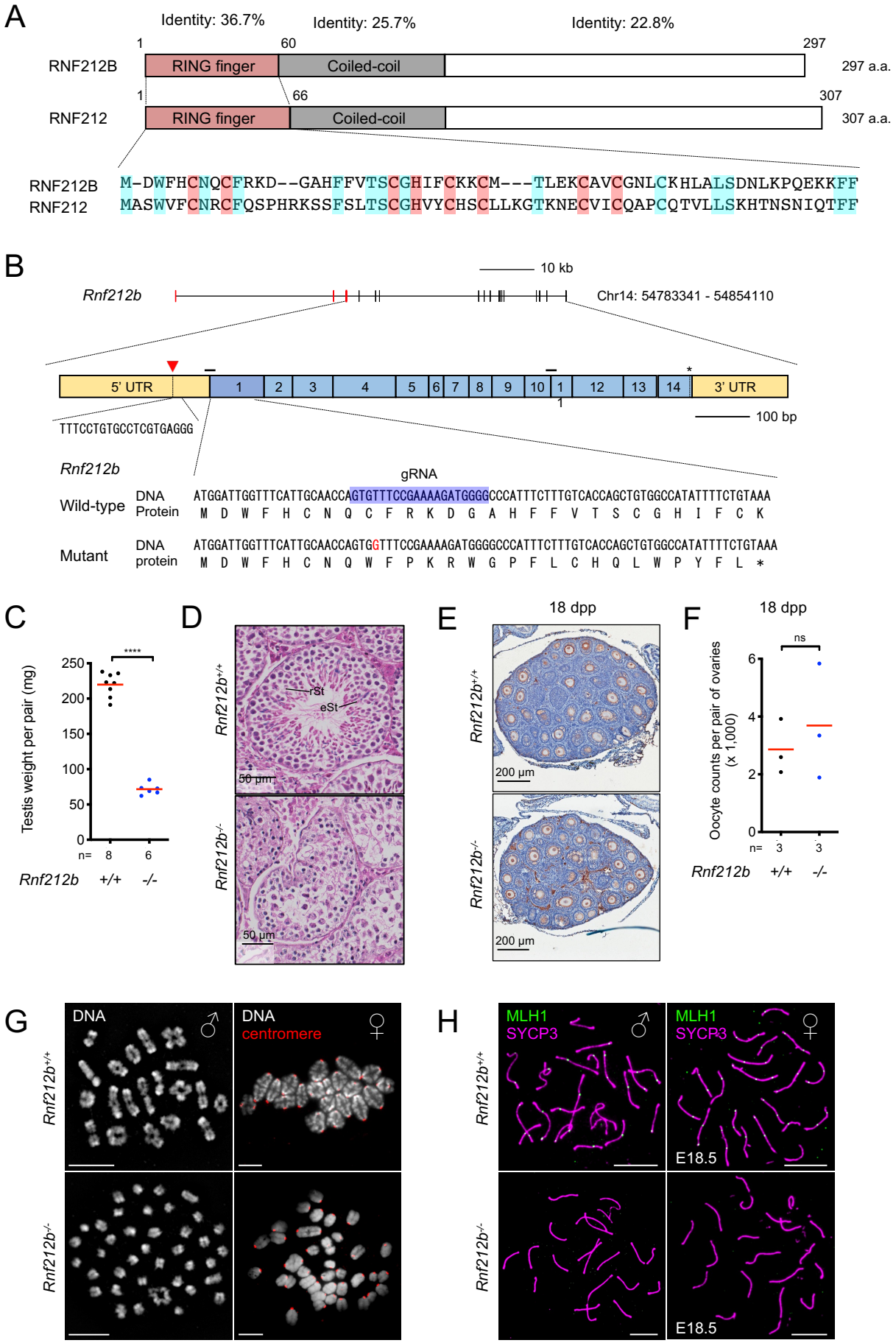

Ito et al., Figure 2

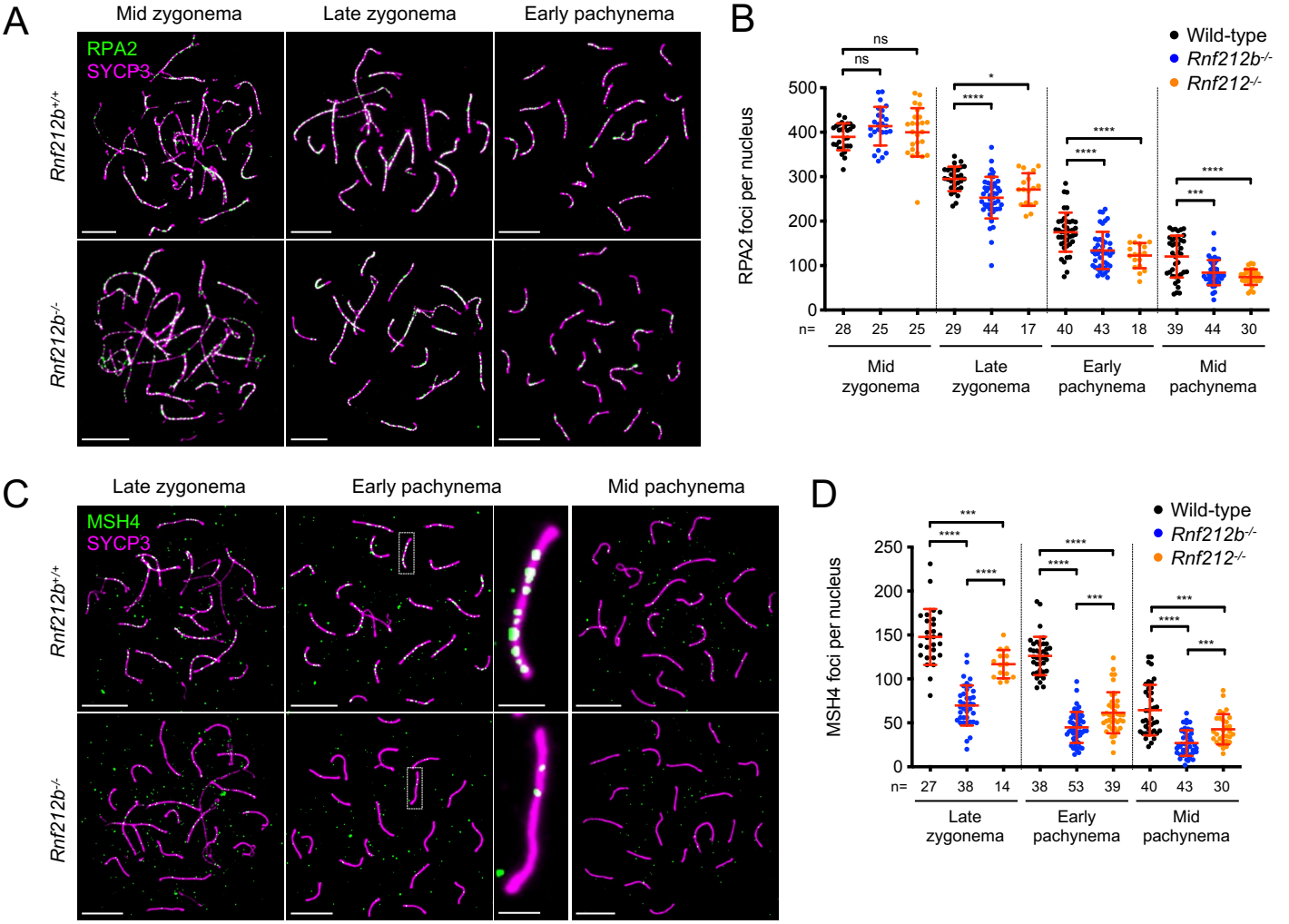

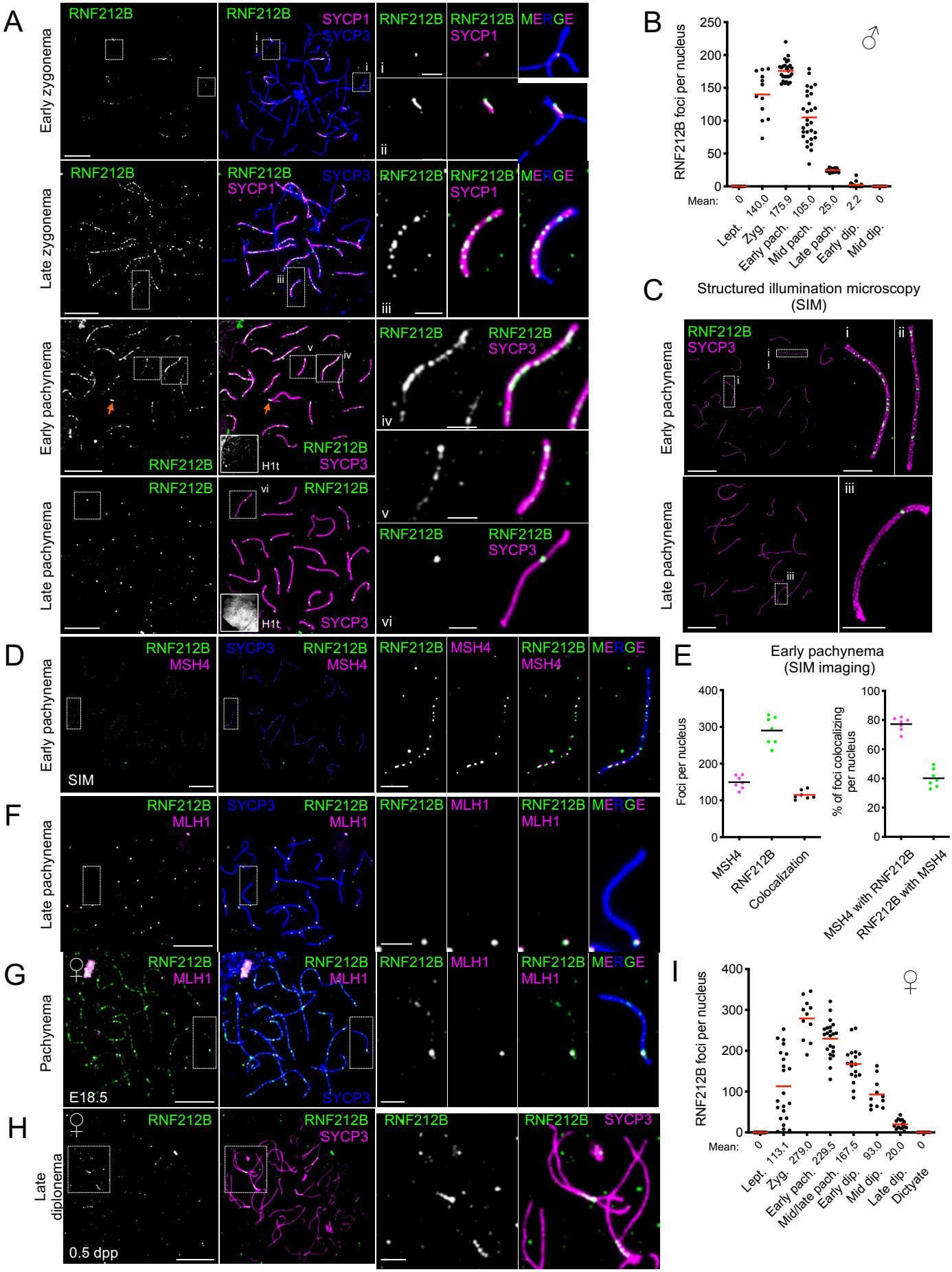

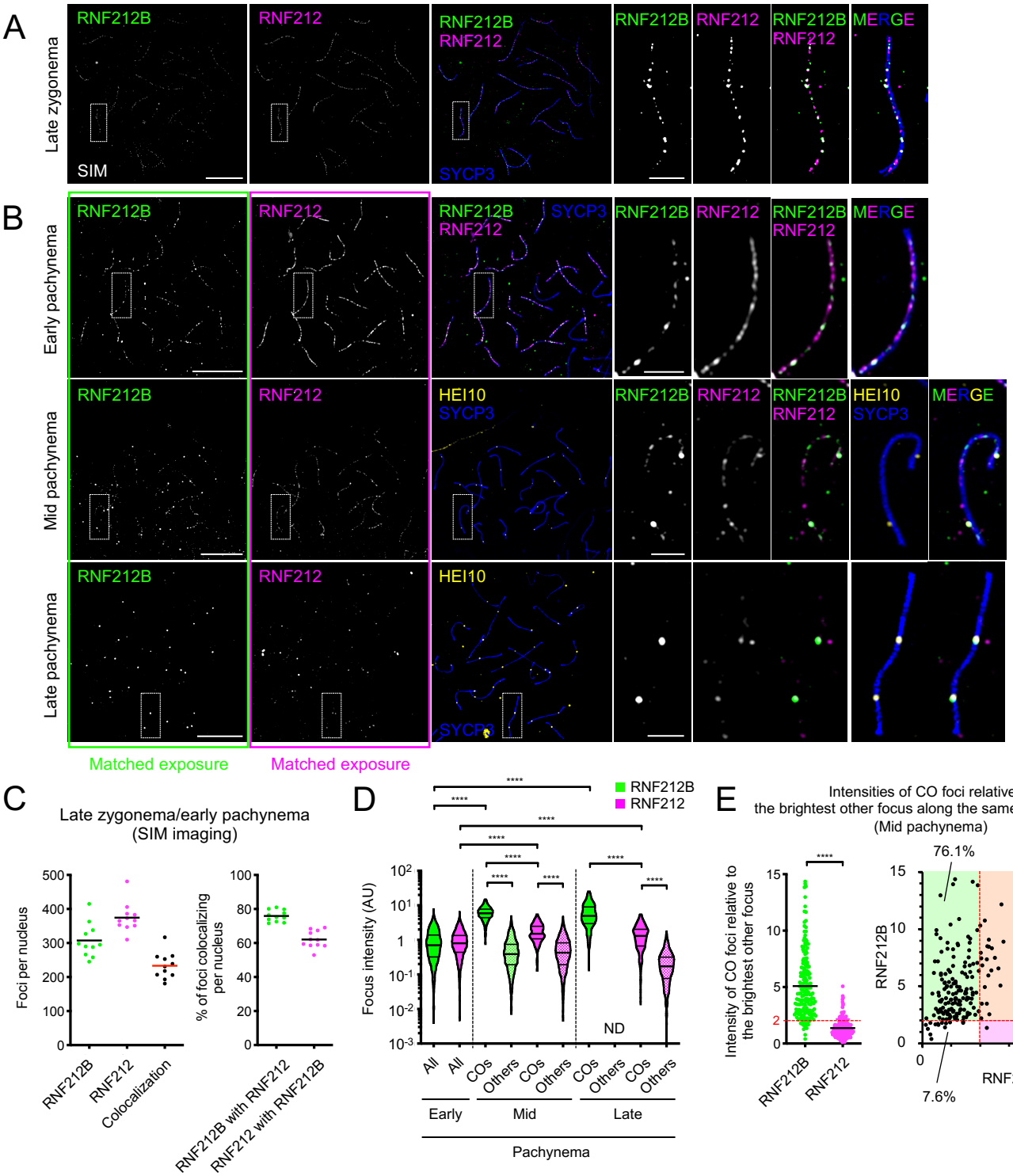

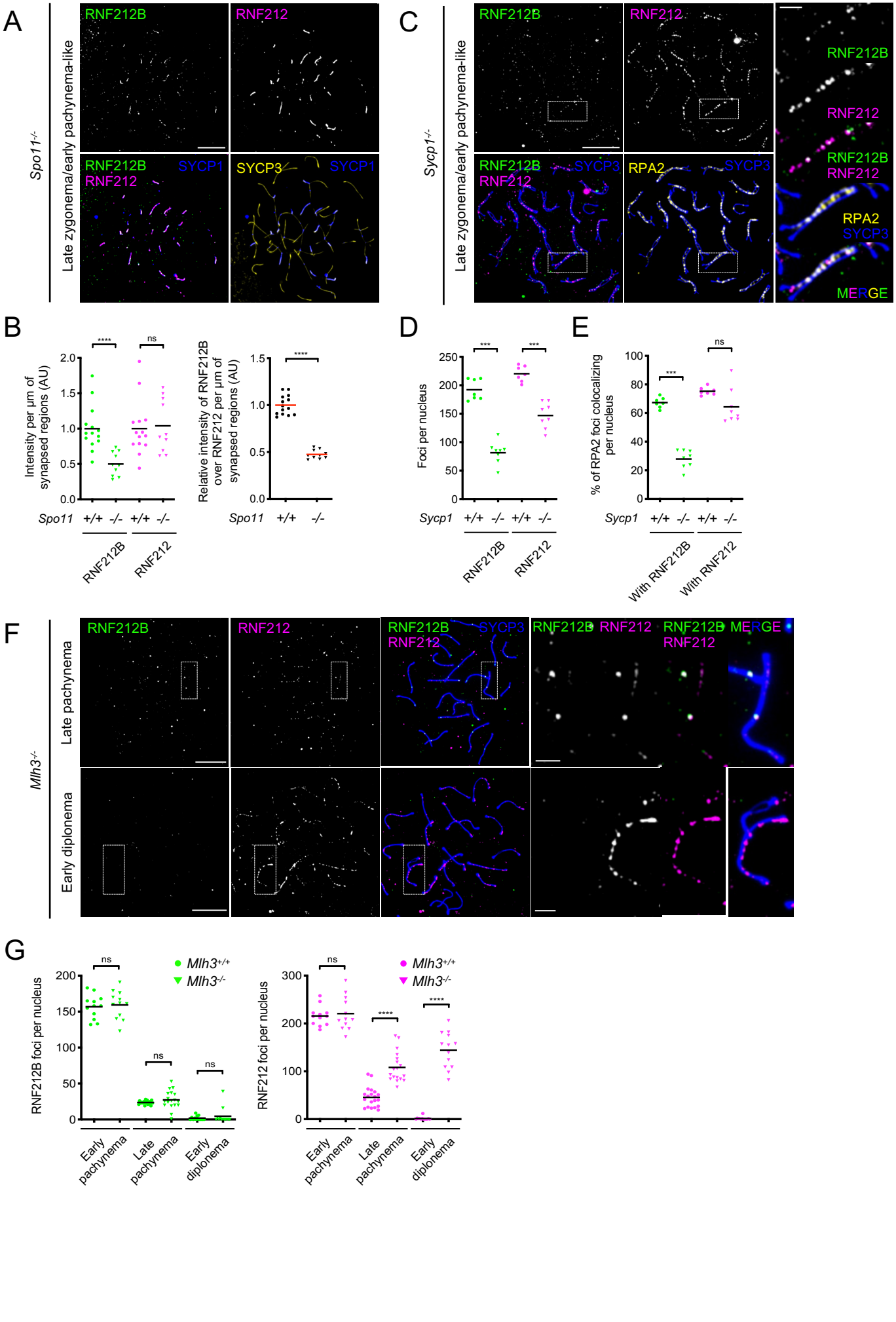

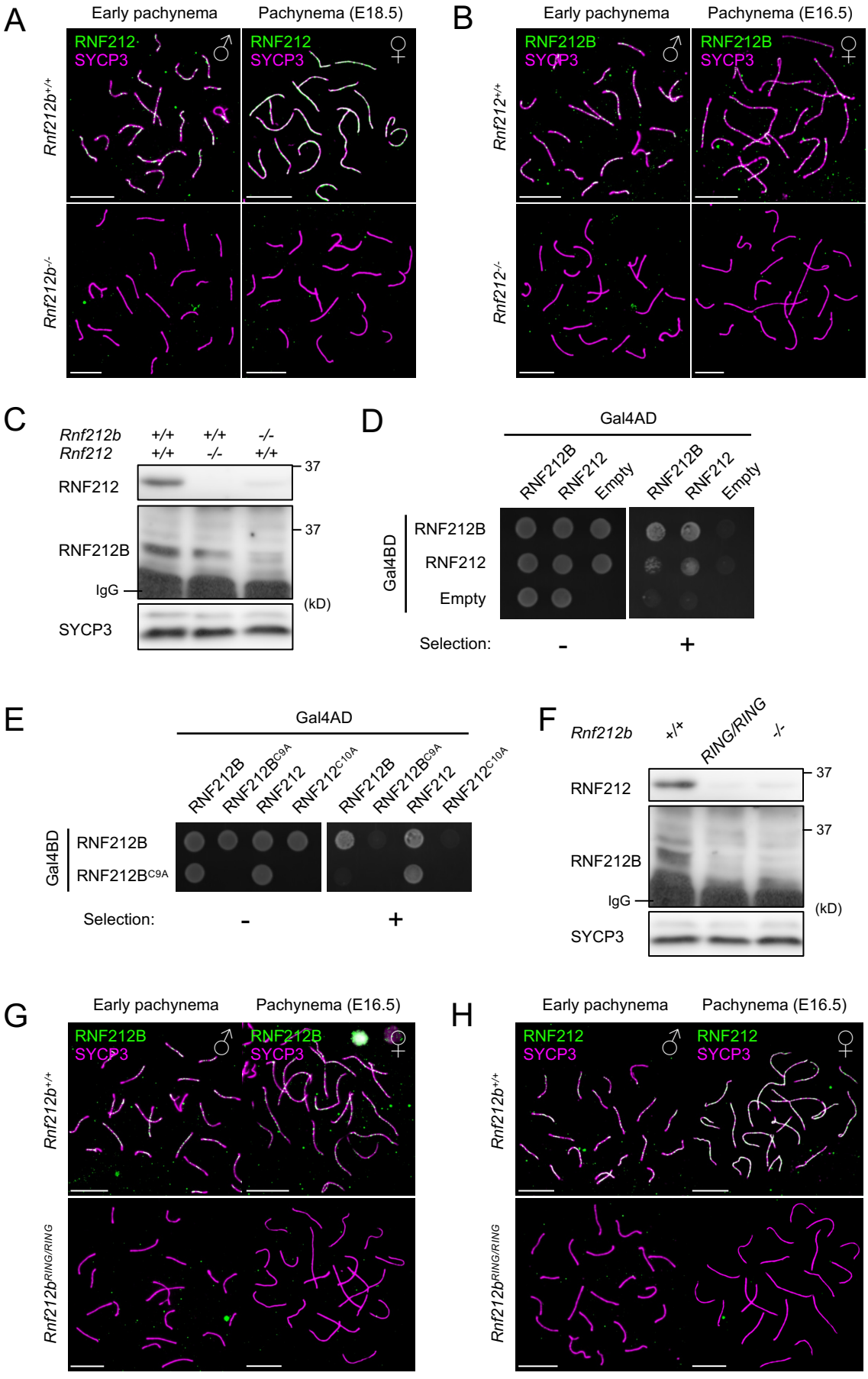

Ito et al, Figure 7